

# **Wire Arc Additive Manufacturing of ER70S-6 Mild Steel with 304 Stainless Steel Interlayer : study Defects and Mechanical Properties**

A Thesis

Submitted by

**AKASH DWIVEDI**

*in partial fulfillment of the requirements for the award of the degree of*

**Master of Technology**

*in*

**Mechanical Engineering  
(Materials Science & Technology)**



Department of Mechanical Engineering  
NATIONAL INSTITUTE OF TECHNOLOGY CALICUT

June 2023

## **ACKNOWLEDGEMENT**

I take this opportunity to express my deep sense of gratitude and sincere thanks to all who have helped me to complete this work successfully. I am deeply indebted to my Course Coordinator and Guide Dr. Jinu Paul for his excellent guidance, positive criticism, valuable comments and suggestions. Dr. M.A Joseph for helping at every stage of the project.

I am grateful to my family and friends, who helped me at hard times. Finally, I express my big thanks to almighty that strengthens me throughout my life.

Akash Dwivedi

## DECLARATION

*I hereby declare that this submission is my own work and that, to the best of my knowledge and belief, it contains no material previously published or written by another person nor material which has been accepted for the award of any other degree or diploma of the university or other institute of higher learning, except where due acknowledgment has been made in the text.*

Signature : Akashdwivedi

NIT Calicut

Name : AKASH DWIVEDI

Date : June 05,2023

Roll No : M210584ME

## CERTIFICATE

This is to certify that the thesis entitled: “**Wire Arc Additive Manufacturing of ER70S-6 Mild Steel with 304 Stainless Steel Interlayer : study Defects and Mechanical Properties**” submitted by **AKASH DWIVEDI** (Roll No.: **M210584ME**) to the National Institute of Technology Calicut towards partial fulfillment of the requirements for the award of the Degree of Master of Technology in Mechanical Engineering (Materials Science and Technology) is a bonafide record of the work carried out by him/her under my supervision and guidance, and this work has not been submitted elsewhere for the award of a degree.

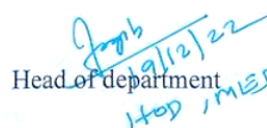


**Dr. Jinu Paul**

(Guide)

*Associate Professor*

*Dept. of Mechanical Engineering*



Head of department  
HOD, ME

*Dept. of Mechanical Engineering*

*Place:* NIT Calicut

*Date:* December 19, 2022

## **ABSTRACT**

Additive Manufacturing (AM) has opened up new possibilities for researchers to fabricate products and has even replaced older techniques in certain industrial settings by reducing material usage. Wire Arc-Additive Manufacturing(WAAM) has gained considerable popularity in the study of additive industry attributable its exceptional efficiency and numerous advantages. This technique offers several key benefits, including high-deposition rates, improved material usage, reduced lead-times, enhanced element efficiency, and decreased inventory capital. Like welding, which is a conventional method, Wire Arc-Additive Manufacturing utilizes a layer-wise deposition approach to construct larger objects with comparatively lower complexity. The attainment of manufacture of the highest calibre in WAAM is impeded by the significant levels of heat input, leading to various processing challenges and defects. This work primarily addresses the common challenges encountered during the fabrication of various metals and alloys using Wire Arc-Additive Manufacturing (WAAM). These challenges encompass elevated residual stresses, porosity, cracking, and delamination. The work also provides an overview of the fundamental aspects of the Wire Arc-Additive Manufacturing method, important steps involved, defects that may arise, and the process planning required for Wire Arc-Additive Manufacturing. Additionally, the results of the research are presented, and the challenges and future prospects in this field are discussed.

# CONTENTS

List of Figures	iii
List of Tables	v
<b>1. Introduction</b>	<b>1</b>
<b>2. Literature Review</b>	<b>5</b>
2.1 Materials used	6
2.1.1 Titanium alloys	6
2.1.2 Aluminium alloys	7
2.1.3 Nickel alloys	7
2.1.4 Steel alloys	8
2.1.5 Bimetal alloys	8
2.2 Geometric aspects	9
2.3 WAAM Process Parameters	10
2.3.1 CAD model parameter	11
2.3.2 Tool Path	12
2.4 Welding process parameter	13
2.5 Defects in WAAM	14
2.5.1 Porosity	15
2.5.2 Residual stress	16
2.5.3 Solidification cracking	16
2.5.4 Fabrication set-up	17
2.5.5 Anisotropy	17
<b>3. Methodology</b>	<b>19</b>
<b>4. Experimental Details</b>	<b>21</b>
<b>5. Results</b>	<b>25</b>
5.1 Micro-structure characterization	
5.1.1 Energy-dispersive X-ray spectroscopy (EDS)	25
5.1.2 Optical Microscopy (OM)	27
5.1.3 Scanning Electron Microscopy (SEM)	29
5.1.4 X-ray diffraction (XRD)	31
5.2 Mechanical Tests	
5.2.1 Tensile testing	33

5.2.2 Micro-hardness testing	36
<b>6. Conclusion</b>	38
<b>7. Future Work</b>	40
<b>8. References</b>	41
<b>9. Appendix</b>	
A-1 To obtain stable and defect-free components for WAAM, welding process parameters to be considered include	45
A-2 Life Cycle of a WAAM part	46

## LIST OF FIGURES

1.1	Metal Additive-Manufacturing techniques	1
1.2	Basic wire arc welding	2
1.3	Schematic diagram of WAAM	3
2.1	(a) and (b) represents the unidirectional build B denotes the Direction as we can see in (b) support is needed whereas in (c) we can see there are 3 build-direction	11
2.2	Various methods of tool path a) Raster, b) Zig-zag, c) Contour, d) Spiral, e) Hybrid	12
2.3	Porosity present in WAAM of Al 2219: (a) CMT; (b) CMT-ADV; (c) CMT-P, and (d) CMT-PADV	15
2.4	The Scanning Electron Microscope (SEM) images shows morphology of tensile metal made from WAAM Al 2219 alloy	17
3.1	Methodology to perform WAAM	19
4.1	WAAM specimen fabrication method	21
4.2	WAAM fabricated specimen	21
4.3	Section of specimen cut from sample	22
4.4	Samples taken from WAAM using EDM	23
4.5	Dog bone specimen for tensile test with dimensions (a) 9.00 mm breadth, (b) 5.00 mm guage breadth, (c) 16.80 mm guage length, (d) 57.00 mm length of specimen	23
5.1	WAAM Mild Steel with and without interlayer Specimen	25
5.2	EDS Characterization to see the composition of WAAM specimen	26
5.3	Dispersion of elements in specimen (a) Electron image, (b) Carbon (green), (c) Silicon (golden), (d) Manganese (blue), (e) Iron (red), (f) Dysprosium (grey), (g) Nickel (cyan), (h) Chromium (violet)	26
5.4	Microstructure image received from Optical Microscope, at resolution of 100µm and 50µm	28
5.5	Grain size and grain area analysis of WAAM specimen with SS interlayer (a) Ferrite region, (b) Pearlite region	28
5.6	SEM images of WAAM specimen without interlayer with resolution of, (a) 20 µm, (b) 50 µm, (c) 100 µm	29
5.7	SEM images of WAAM specimen with 304 Stainless steel interlayer with resolution of, (a) 20 µm, (b) 50 µm, (c) 100 µm	30
5.8	Comparison between WAAM sample with and without interlayer to analyse porosity	31
5.9	Plot of data received from XRD	32



5.10	Tensile test result for WAAM specimen with SS interlayer along horizontal, vertical, and diagonal directions	34
5.11	Tensile test specimen (a) dimensions of the specimen, (b) fractured specimen with cup and cone fracture, (c) specimen under load in UTM	34
5.12	Comparison of WAAM specimen with and without interlayer	35
5.13	Vickers microhardness test for the WAAM specimen with SS interlayer and without interlayer	36
6.1	Comparison of Ultimate tensile of the WAAM specimen along three directions	39
A-I	Graphs between (a) Wire-feed rate vs bead height, (b) Wire-feed rate vs bead width	45
A-II	Graphs between (a) Travel-speed vs bead-width, (b) Travel-speed vs melt-through depth	45
A-III	Graphs between (a) Weld-current vs bead width, (b) Weld-current vs melt-through depth	45
A-IV	Life -cycle of the WAAM specimen	46

## **LIST OF TABLES**

4.1	Parameters used in specimen fabrication	22
5.1	Density and mass of the samples	25
5.2	Composition of WAAM specimen with SS interlayer	27
5.3	Analysis of Porosity present in WAAM samples	31
5.4	Planes corresponding to peaks of XRD	33

# 1. INTRODUCTION

At the forefront of technology, Additive Manufacturing (AM), is an advanced manufacturing process. Someone can consider it as a revolutionary discovery in the industry. Additive Manufacturing also called 3D printing and in industry it is also referred it as rapid prototyping. So the idea behind additive manufacturing is building a product layer wise, one layer at a time using material in powder form or wire form over a predefined tool path given by the computer for that product. In the 1980s, 3D Systems Inc. achieved a significant milestone by becoming the first company to produce a product using a CAD model through a layer-by-layer additive-manufacturing process[1].

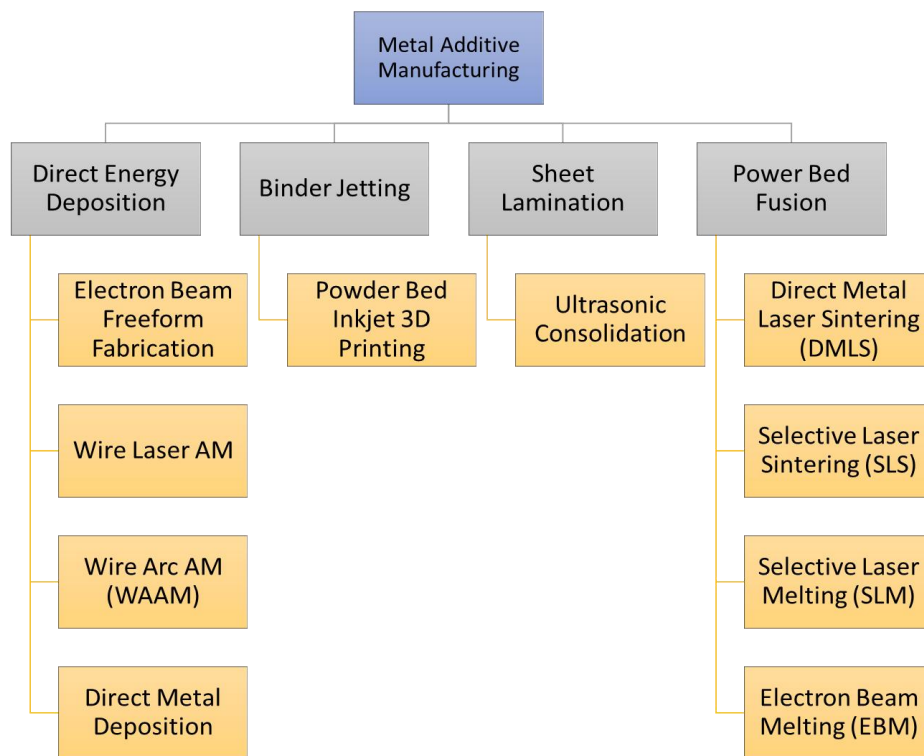


Figure 1.1. Metal Additive-Manufacturing techniques

The reason it is so famous in the industry is because of its tremendous advantages over the conventional manufacturing techniques. The biggest advantage is that it does not require any external tools such as casting moulds, dies and punches. AM allows complex and precise product to be made as per the requirement of the customer. As compared to its counter technique Subtractive Manufacturing (SM) it require negligible additional material therefore little to none material waste. AM's other advantages include it minimizes the time required for

the production [2,3] and since it is providing less material wastage so we can use it to make products which were expensive to make when they were made by conventional techniques [4-9].

The material extrusion and material jetting is mainly used in manufacturing polymer based product. Binder Jetting and Sheet Lamination both of these process can be used to make products from polymer, ceramics, metals and composites. For metal additive-manufacturing, Powder-Bed Fusion and Direct-Energy Deposition(DED) are the commonly utilized techniques [10]. Among these, Wire Arc-Additive Manufacturing (WAAM) is widely used in the production. For process to be used in Industry should have high deposition rate but also should be economical.

In 1920, Baker Ralph employed an electric arc to melt metallic wire and create an ornament, marking the initial application of Wire Arc-Additive Manufacturing [12]. Since then, continuous progress has been made to refine and enhance the WAAM process.

To understand WAAM, It's crucial to have a foundational knowledge of wire-arc welding. Arc-welding is a technique that employs an electric-arc to generate heat, which allows for the melting and fusion of metals. This method involves utilizing a electricity source for starting an electric arc between two electrodes, which can be non-consumable or consumable, and the base material. The power supply can operate with either AC (alternating current) or DC (direct current).

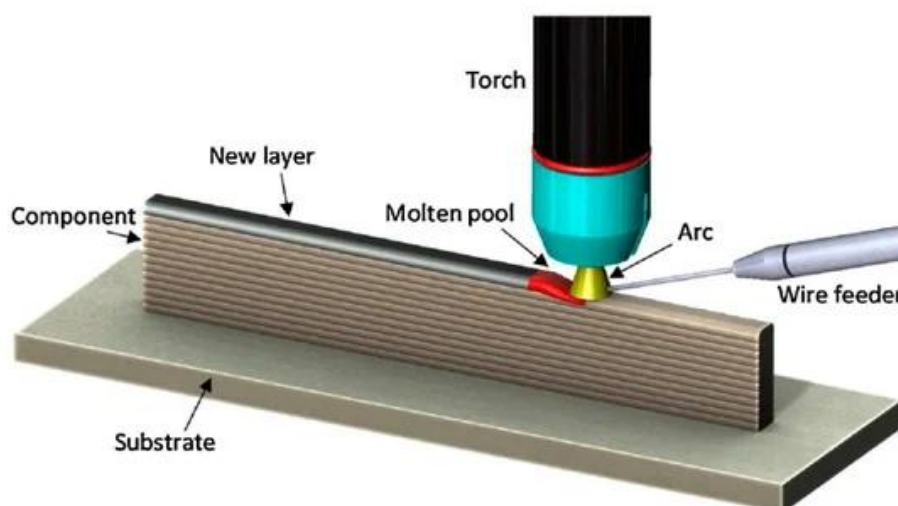


Figure 1.2. Basic wire arc welding [13]

According to the type of energy source used, Arc-welding is divided into several categories. Some of these types include Plasma-Arc Welding (PAW), Gas-Tungsten Arc Welding (GTAW), and Gas-Metal Arc Welding (GMAW). The principles utilized in Wire Arc-Additive Manufacturing (WAAM) are indeed related to those employed in arc-welding. In fact, the primary types of arc welding, such as Plasma-Arc Welding (PAW), Gas-Tungsten Arc Welding (GTAW), and Gas-Metal Arc Welding (GMAW) is another commonly utilized method in Wire Arc-Additive Manufacturing (WAAM), catering to different user preferences and application needs. In WAAM we melt the wire but instead of joining metals (like in arc welding), we let the molten bead fall on the pre-defined path layout and after we repeat this process multiple times we would have a stack of molten beads melted together in the specific layout creating a additive manufactured product. Apart from the process planning and execution of these processes, they also differ in a basic thermal conductance to the metal and surrounding, which is found by Cunningham, Mohebbi et al.[13].

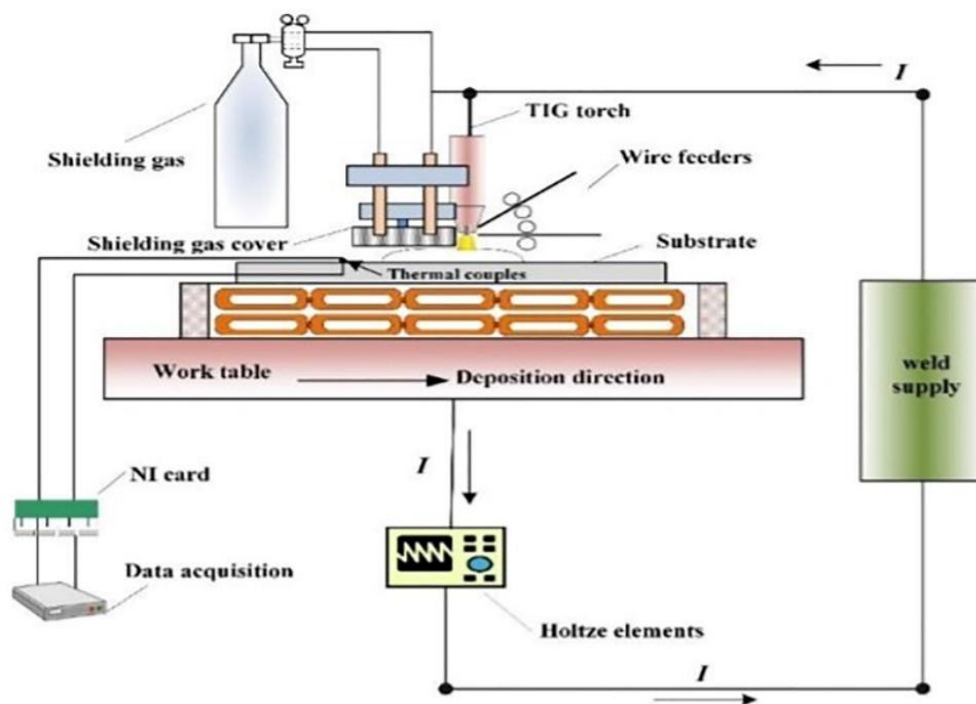


Figure 1.3 Schematic diagram of WAAM

So in WAAM the energy lost by the melted bead is mainly to the layer below it, thus melting and joining to the layer below it. In the additive-manufacturing process, every layer is sequentially placed on top of the preceding layer. During this process, the material undergoes repeated cycles of heating and cooling, ultimately leading to the creation of unique and final

net shape parts. An important benefit of this approach is that it eliminates the need for additional tooling processes[14].

Process planning is a major aspect of WAAM. To understand it we must first define major WAAM components. Figure 5 presents the fundamental schematic of the Wire Arc-Additive Manufacturing process [15]. To enhance comprehension, let's divide WAAM into three distinct parts: process-planning, depositions, and post processes. During process planning, the initial step involves creating a CAD model of the desired product. Then this 3D model is sent to a software to be converted into 2D layers of thickness according to requirement. After this a programme would make a layout according to these 2D layers.

After the program is prepared, it is transferred to a CNC machine. The CNC code is generated based on this program. Furthermore, in Figure 3, there are multiple sensors, such as cameras and thermocouples, which are utilized to gather real-time data during the melting process. This data includes information on the table speed, material feed rate, gas flow rate, arc current, heat input, path strategy, and more. These data are then feedback to the computer to generate new process parameter values which can give more accuracy to the product. Hence it explains the closed circuit loop in the figure 3.

The process planning makes WAAM little complicated than the conventional. Moreover, the materials which we can use in WAAM is very limited right now. Researchers are testing new materials and conducting experiments to reduce the defects in the product so that they are industry ready. Some of the common materials are aluminium alloys, titanium alloys, nickel based alloys and steel based alloys etc. more details can be found later in this paper.

As there are many parameters which are directly related to the manufacturing of the product, this will inevitably make it more vulnerable to defects. Later in the paper, defects such as cracking, porosity, and residual stress are thoroughly discussed. The paper also explores geometry and its relationship to particular parameters of the fabricated part in subsequent sections. Many post processing methods has also been researched that can reduce the defects to such an extent that their properties even extend the properties of the same product manufactured by conventional ways.

## 2. LITERATURE REVIEW

A element is constructed using the layer approach of WAAM instead of subtractive manufacturing methods. This results in improved material efficiency and cost-effectiveness since the material is selectively deposited only where it is required. By employing the WAAM process, the production of parts is streamlined, significantly reducing the need for additional machining due to the attainment of close-to-final shape components. Compared to products manufactured using traditional subtractive methods, WAAM components exhibit favorable density and high mechanical properties. Additionally, WAAM can be utilized for repairing structures and parts such as bridges, turbine blades, molds, and dies. Worn-out parts can be restored by depositing new material onto their surfaces using WAAM, eliminating the need for additional raw materials and processes, leading to significant cost savings. Furthermore, WAAM demonstrates a deposition rate that falls within the range of 10 to 130 g/min, surpassing the deposition rates achieved by additive manufacturing techniques that employ laser power sources or electron beam (2-10 g/min) [28]. Within the WAAM process, an electric-arc generated by a power supply unit serves as the energy source. This electric arc induces the liquefying of the electrode wire, resulting in the formation of a liquid metal pool. By carefully selecting suitable welding settings and tool paths, it becomes possible to fabricate products with desired shapes and sizes. The planning and construction of the tool path are designed to efficiently produce higher volume shapes or components with slightly less complex forms.

WAAM utilizes three primary electric arc types: MIG, TIG, and PA. Among these, MIG is the most commonly used method due to its shorter tool path and the use of wire as a consumable electrode, which is aligned with the melting source. In contrast, Tungsten-inert Gas (TIG) and Plasma-Arc welding (PAW) techniques necessitate the introduction of an external wire into the melt pool since the electrode used is not disposable. In such cases, programming the torch for consistent deposition becomes more challenging because it requires rotation to enable continuous feeding of the wire from the same direction. [29]. During the Metal Inert Gas (MIG) welding process, the arc causes molten metal to be transferred from the consumable electrode, which may lead to the expulsion of molten droplets. This phenomenon results in spatter and the formation of surface balling. Unlike other welding methods, such as Metal-inert Gas, Tungsten-inert Gas and Plasma-Arc welding

processes do not encounter spatter. This phenomenon occurs due to the direct supply of filler metal to the weld pool in these processes [30]. In the case of aluminum and steel feedstocks, the Cold Metal Transfer variant of MIG is well-suited. The CMT technique utilizes a mechanism known as controlled dip transfer mode, which allows for the production of high-quality beads with minimal spatter and reduced heat input. The finer grains achieved through reduced heat input can enhance mechanical characteristics [27]. Unlike standard MIG, CMT synchronizes the mechanical motion of the wire with the electrical process control, which monitors parameters such as thermal input, short-circuiting phase, and arc length [28]. For more detailed information, refer to references [27-29]. When considering the size of construction parts, a high deposition rate is crucial to ensure timely fabrication. For this reason, MIG (Metal Inert Gas) welding is preferred in the construction sector due to its higher deposition rate, which can reach several kilograms per hour. In contrast, TIG (Tungsten Inert Gas) welding typically achieves an approximate deposition rate of one kilogram per hour. [27]. Consequently, earlier research on WAAM construction has predominantly focused on MIG, which might have limited the exploration of its potential applications. Civil engineers should also explore different variants of WAAM for various structural applications. For example, TIG (Tungsten Inert Gas) welding can be utilized when higher geometric accuracy and improved surface finish are required [27], while PA (Plasma Arc) welding can be employed to produce parts with a larger deposition width compared to MIG (Metal Inert Gas) welding [30].

## **2.1 Materials used**

A broad range of spooled wires, which are commonly used in the welding industry, can be readily utilized as feedstock material for the WAAM process. The availability of wires in diverse alloys is vital as they have a great significance in ensuring the production of defect-free and dependable parts. Having a solid understanding of the available processes, process control variables, key concepts, and input materials is essential. Table 1 presents a compilation of frequently employed alloys in WAAM along with their respective applications. In this part of the article, we will explore the metals generally considered in the WAAM technique.

### **2.1.1 Titanium alloys**

Extensive research has been done to inspect the use of titanium alloys in various industries using WAAM technology. This focus arises from factors such as the difficulties in machining, the comparatively higher cost of materials, and the advantageous ratio of strength to weight



exhibited by titanium alloys. In WAAM, the deposition rates for titanium alloys typically range from 0.75 to 2 kg/hour. Additionally, the typical values for resolution, surface-roughness (including surface waviness) are about 0.5 mm. As a result, the resulting metal layers exhibit high density, eliminating the need for additional processes like Hot Isostatic Pressing (HIPing). Moreover, the size of the component that can be produced is solely restricted by the reach of the manipulator. [39]. Notably, WAAM-deposited Ti-6Al-4V exhibits improved damage tolerance properties, particularly when subjected to heavy cyclic loads, surpassing the performance of the wrought alloy by one order [40]. However, it is important to consider that titanium alloys demonstrate significant anisotropy in terms of elongation and tensile strength. The rolling process induces strains in the component in both the transverse and normal directions [41,42].

### **2.1.2 Aluminium alloys**

Successful fabrication trials have been conducted on various series of aluminum alloys, including Aluminum-Copper (2xxx), Aluminum-Silicon (4xxx), and Aluminum-Magnesium (5xxx). While conventional machining costs tend to be lower for simple and small components, WAAM technology proves to be economically feasible for complex parts with large and thin walls [43]. However, it is essential to acknowledge that there is a disparity in the mechanical properties between deposited aluminum alloy parts and billet aluminum alloy parts. To improve the strength, properties, and microstructure of aluminum parts, post-process heat treatment is necessary. The welding of alloys such as Al7xxx and 6xxx poses challenges, mainly due to the occurrence of weld-defects and the generation of a turbulent melt-pool while deposition process, which restricts the application of aluminum in this technique. The most common flaw encountered in deposited aluminum is "porosity." To mitigate porosity, it is crucial to optimize synergistic operating parameters and employ high-quality feedstock wires.

### **2.1.3 Nickel alloys**

Nickel-based superalloys are in high demand for additive manufacturing (AM) due to their exceptional capability to maintain high strength even at elevated temperatures. Conventional fabrication methods for these alloys tend to be expensive, which has led to the widespread adoption of the WAAM technique for commercial applications. Among the different alloys based on nickel, significant attention has been drawn to Inconel 625 and Inconel 718, which have been extensively studied in numerous research investigations to understand their

properties. Concerning microstructure, WAAM-produced Inconel 718 exhibits distinct columnar grains distinguished by dendritic boundaries [44]. The ultimate strength, yield strength, and ductility of deposited nickel alloys typically exhibit similar or slightly lower values equating to that of wrought or cast materials [45].

#### **2.1.4 Steel alloys**

The high ductility and corrosion resistance of stainless steel make it an attractive material for fabrication using the WAAM technique, leading to numerous investigations in this field. Research studies have shown that WAAM technology can generate stainless steel components with favorable mechanical property and micro-structure [46]. During welding or deposition processes, the micro-structure of stainless-steel is predominantly austenitic, consisting of both austenitic and ferritic phases [47]. The phase fraction of stainless steel is affected by several factors, such as the thermal cycle experienced during welding or deposition and the chemical content of the element [48]. The rate at which the material cools down after welding or deposition is a significant factor in determining the content of ferrite in the final part. By controlling the cooling rate, it is possible to achieve a volume fraction of up to 30% ferrite [49, 50]. Choosing the right process parameters is crucial in order to attain a well-balanced microstructure in stainless steel. These parameters directly impact the outcome and help achieve the desired properties and characteristics of the element. Faster cooling can result in precipitation of non-equilibrium nitrides and a restricted formation of austenite [51,52]. Although components may exhibit slight anisotropy, this can be eliminated through suitable post-process heat treatment, resulting in properties similar to those of conventionally produced products. WAAM-deposited stainless steel parts are extensively employed in the manufacturing of high-performance alloy components [48].

#### **2.1.5 Bimetal alloys**

Extensive research has been conducted to evaluate the viability of a broad spectrum of metals for Wire Arc-Additive Manufacturing (WAAM). These investigations encompass bimetallic combinations such as steel/nickel and steel/bronze, as well as magnesium alloys. Moreover, alloys frequently used in aerospace applications, such as Fe/Al and Al/Ti, as well as in the automotive industry, have also undergone extensive examination and analysis. These alloys are being examined due to their unique properties and potential for various engineering applications. [45]. The main aim of the investigation has been to assess the mechanical and

microstructural properties, particularly for simple parts with straight walls, rather than placing significant emphasis on the overall advancement of the process for manufacturing functional components.

## **2.2 Geometric aspects**

Unlike other additive-manufacturing processes, Wire Arc-Additive Manufacturing (WAAM) techniques are widely recognized as high deposition rates can be achieved. This characteristic sets WAAM apart from other methods in the field of additive-manufacturing. However, it is important to keep in mind that Wire Arc-Additive Manufacturing (WAAM) techniques, while offering higher deposition rate, are often associated with lower part precision compared to other additive manufacturing processes. As a result, research efforts have predominantly focused on addressing geometry control as a crucial area of interest in WAAM [27, 28]. Investigations into dimensional control, encompassing the height and width of each layer, have been conducted for various metallic materials [27, 28]. Parameters such as the thickness of the wire and various process variables, including wire-feed speed, heat input, and travel speed, have a significant impact on the wall-thickness and deposition effectiveness achieved during a single pass deposition. Commonly used wire sizes for constructing materials like stainless steel and carbon steels ranging from 0.8 mm to 1.2 mm. The use of these wire sizes leads to section thicknesses that typically ranging from 3.5 mm to 8 mm for a single pass wall [36, 29, 30]. Thus far, the majority of WAAM builds in construction applications have utilized single-pass walls with consistent thickness [35]. Nonetheless, achieving thicker walls can be accomplished by employing multiple wire feeds and printing passes, introducing complexities to path planning [37].

A ground breaking hybrid directed energy deposition (DED) technique [38] has been developed, which combines laser and plasma transferred arc (PTA) as the primary energy sources. This innovative hybrid process enables precise modulation of wall thickness, offering smoother control over geometry. Furthermore, it offers considerably higher deposition rates in comparison to pure arc or laser-based AM processes. [38]. Further exploration of different combinations of energy sources holds promising research possibilities to meet diverse objectives [60].

Relying solely on traditional welding criterion, consisting arc-current, arc-voltage, wire-feed speed, shielding gas flow, and travel-speed monitoring, is inadequate for comprehensive control as these parameters primarily pertain to the system rather than the specific component itself. Consideration of additional environmental factors, such as heat build-up, is necessary to address potential flaws and their detrimental effects. Various monitoring modalities, including thermal signal, optical signal X-ray CT, and acoustic signal, have been described in [33]. Effective inspection are crucial for in-situ detecting defect and it's prevention. [33].

The precision of WAAM components largely depends on accurately predicting and controlling the dimensions of each layer, which are influenced by multiple process parameters and their cumulative effects. Early digital modeling approaches, such as the one proposed by Ding et al. [34], employed finite element analysis to simulate the thermo-mechanical properties of many layered wall construction during the WAAM. This approach allowed for the estimation of accumulated deformation and residual stress. Xiong et al. [35] investigated the use of neural network modeling for predicting deposition geometry and optimizing process parameters in GMAW-based WAAM. Digital modeling techniques have significantly enhanced confidence in geometric control and residual stress analysis of WAAM parts. Nevertheless, the impact of process factors can differ across various materials, posing challenges in collecting and leveraging process knowledge from extensive literature. To overcome this, digital technology and machine learning [36] can be utilized to optimize process parameters and attain the desired geometry. The development of a computerized tool for data collection from diverse literature sources, as demonstrated in [36], has shown potential in data-driven process control for additive manufacturing.

### **2.3 WAAM Process Parameters**

WAAM allows for the production of products with the desired shape and acceptable surface roughness. However, it is necessary to machine finish the end product before it can be utilized in the industry. But the post processing process can be minimized if the product is made with the accurate processing parameter. The processing parameter plays the major role in deciding quality of the product. In this section we will discuss about the main parameters which affects the product directly.

### 2.3.1 CAD model parameter

The initial stages of manufacturing a 3D product involve preparing a CAD model and performing 2D slicing of the CAD model to generate tool paths. It is helpful to get the model in “.stl” file format because it would be then easy to slice it in 2D layer [39]. There are mainly two type of slicing available unidirectional slicing and multidirectional slicing. In most of the applications unidirectional slicing is used because it relatively simple. However, a drawback of unidirectional slicing is the need for numerous support structures when dealing with complex and overhanging structures. On the other hand, multidirectional slicing (MDS) does not require as much support. As a result, modern AM machines are increasingly utilizing MDS. In MDS, the slicing process is performed in a manner that allows the multi-axial robot to deposit each layer in any orientation [40,41]. Since MDS require such complex algorithms to control the nozzle and the orientation of the robot, that’s why it requires complete robotic configuration [42]. An example of unidirectional vs multidirectional slicing is showed in figure 4.

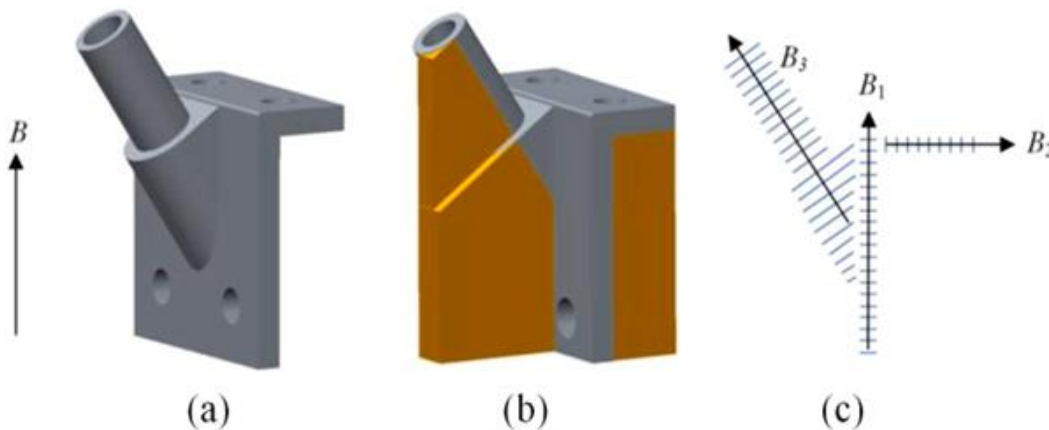


Figure 2.1. (a) and (b) represents the unidirectional build B denotes the direction as we can see in (b) support is needed whereas in (c) we can see there are 3 build-direction that is B1, B2 and B3 [40],[41]

### 2.3.2 Tool Path

This is crucial step in ensuring the production of a high-quality 3D printed product as it guides the nozzle to deposit the melted bead on the 2D layout got from the slicing process. The type of deposition technique used affects the property of the product. Moreover, there is always some mathematical uncertainty in routing path that can also affect the property of the product.

There are many types of tool path that we can program the nozzle to follow, some of which are discussed below

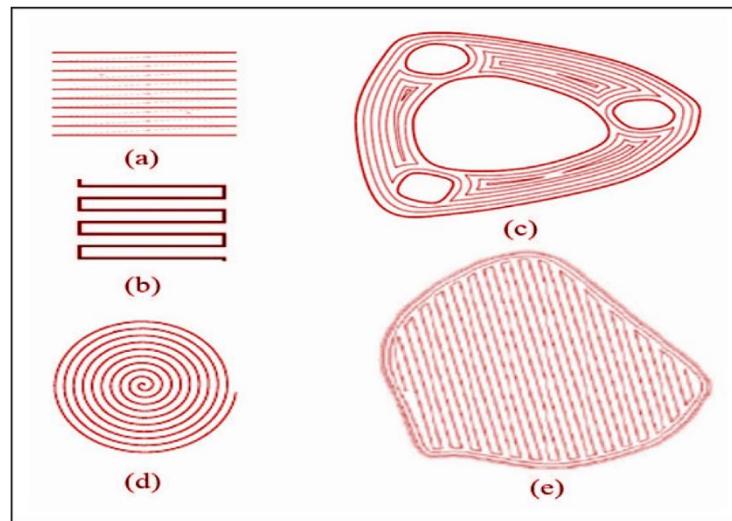


Figure 2.2. Various methods of tool path a) Raster, b) Zig-zag, c) Contour, d) Spiral, e) Hybrid [43],[44]

a) Raster: as seen from fig 5. (a), in raster straight parallel beams is used to cover the contour. It is discontinuous that means when it deposits one layer it goes back to the same side it started and then offsets downwards by pre-programmed distance and starts depositing again parallel to the first layer. It is simple and sufficiently can be used in any boundary therefore more frequently used than other tool paths [44].

b) Zig zag: it is similar to Raster but instead it is continuous as we can see from fig 5(b). therefore, reducing the tool path. The raster and zig zag both have same disadvantage, and that is, at boundary of the layout If the layout at the edge is not uniform and moreover if it is not in the path of the depositing layer, then we will not get the accurate results. Thus both have poor accuracy [45].

c) Contour: as shown in fig 5 (c) contour path overcome the disadvantage that raster and zig zag had. It follows the layout of the outer boundary for depositing the layer and thus eliminating the boundary problems. The inner part is filled based on the outer boundary, as illustrated in the figure 5 (c) [46].

d) Spiral: spiral tool path as shown in fig 5 (d) it eliminates any boundary problems but it can be applicable to some specific geometric shapes only.

e) Hybrid: out of the four tool paths discussed above zig zag is the most economical but if see the accuracy wise the contour is the best. In the industry we need the path which is both

economical and also should give high accuracy. Solution of this problem is to use multiple tool path like the one shown in fig 5 (e). it shows the boundary is done by following contour path and the inner side of the layout is done by zig zag path. Therefore, this path is most suitable for industry use.

## **2.4 Welding process parameter**

As we have established, the precise shape and size of the basic bead are crucial for achieving a high-quality 3D printed product. This property relies on essential parameters including electric current, wire-electrodes extension, wire-feed speed, welding speed, and supply voltage. These parameters vary based on the material and the specific type of product being produced. Below are specific examples that illustrate how different parameters can affect various materials in different scenarios. A study carried out by Malcolm Dinovitzera and his team in 2019 [49] explored the impacts of process parameters in TIG-based WAAM. It was observed that during the solidification of the weld pool, several interfacial defects formed on the substrate. The travel speed and current were identified as the main factors influencing the bead microstructure and overall surface properties. Raising the wire feed rate led to an elevation in the height of the bead. However, melt-through depth and surface roughness were not influenced by the wire feed rate. Bead width and melt-through depth showed an inverse relationship with travel speed, indicating that higher travel speed led to narrower bead width and reduced melt-through depth. Travel speed was found to be inversely proportional to heat input, meaning that higher travel speed resulted in lower roughness. The study also found that the distance from the substrate influenced the microstructure, resulting in the presence of three distinct zones across the multiple layers. In columnar grain matrix adjacent to the bead substrate interface, the first zone displays the presence of finely dispensed carbides. In contrast, the second zone displays larger carbides with a less uniform distribution compared to the first zone. However, in the third zone, a fine and even distribution of carbides was restored within a cellular grain structure.

In a study conducted on Ti6Al4V alloy, it was observed that the bead structure varied with increasing height until a certain point, after which the differences became insignificant. These variations were attributed to changes in the heat dissipation route [52]. The microstructure and grain size of Ti6Al4V were found to change along the construction direction. The optimum temperature for achieving the best mechanical properties was

determined to be 2000°C [53]. It was also noted that a lower wire feeding angle (30°-40°) resulted in cracking [54]. In a study performed by Evangeline et al. [55], it was observed that the width of a weld bead was directly related to the welding current. This relationship was attributed to the increased welding current magnitude applying additional pressure on the droplet of the molten metal, which resulted in the formation of a wider bead. The steady welding current, combined with an increase in welding speed, contributed to this relationship.

## **2.5 Defects in WAAM**

Significant efforts have been dedicated to addressing the challenges associated with the manufacturing of products using WAAM technique. The fabrication of components using the WAAM technique presents several challenges that have been addressed through ongoing research and development. These challenges encompass various aspects of the process, including programming, control of deposition parameters, weld pool dynamics, thermal deformation, machine reliability, and environmental considerations. Additionally, specific materials used in WAAM can introduce their own set of issues. For instance, titanium alloys may experience oxidation, aluminum alloys can exhibit porosity, steel components may encounter significant deformation and surface roughness problems, and bimetal parts may be susceptible to crack formation. This section focuses on discussing these issues in relation to the materials involved. In industries such as aerospace and automotive, Welding Arc-based Additive Manufacturing (WAAM) techniques are preferred over traditional subtractive manufacturing and other methods for fabricating intricate product structures. However, the difference in micro-mechanical properties of the WAAM made products remains a significant challenge. This is mainly attributed to factors such as the stair-step effect, residual stress, porosity, and solidification cracking. Figure 16 illustrates that specific defects tend to be more prominent in certain materials. For instance, severe oxidation is observed in titanium alloys, porosity is common in aluminum alloys, steel often exhibits poor surface roughness, and bimetal components are susceptible to severe deformation and crack formation.

### **2.5.1 Porosity**

Surface contaminants, including grease, moisture, dust particles, and hydrocarbons, present in the raw materials such as the substrate and feedstock wire, can be absorbed into the molten pool throughout the WAAM process. This absorption results in formation of porosity during solidification, with aluminum alloy being particularly susceptible to this challenge. The



presence of a small volumes of dissolved hydrogen in the liquid form might transcend the optimal solubility, resulting in the formation of porosity in the final part. Therefore, it is crucial to thoroughly clean the raw materials, especially aluminum alloys. The occurrence of porosity induced by the process is primarily caused by unstable deposition, insufficient shielding, and inadequate path planning. There are several methods available to control porosity in WAAM:

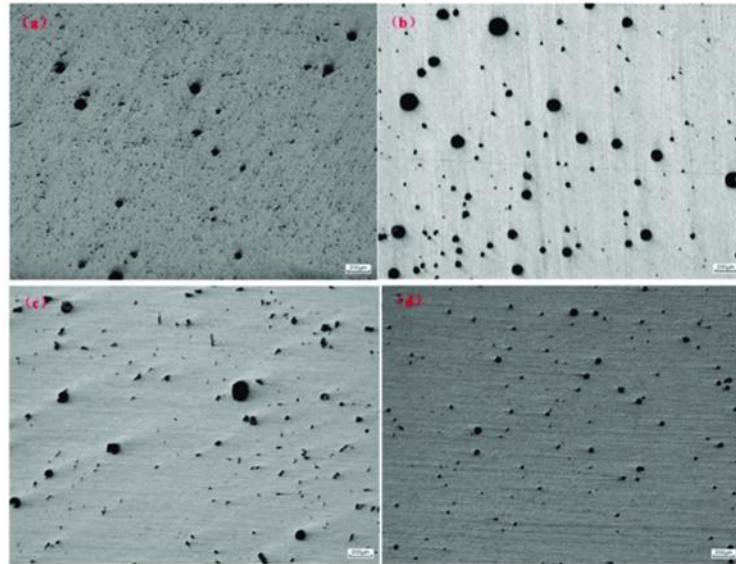


Figure 2.3. Porosity present in WAAM of Al 2219: (a) CMT; (b) CMT-ADV; (c) CMT-P, and (d) CMT-PADV

1. Utilizing a cold-metal transfer sourced GMAW or controlled short circuit process (CMT-PADV).
2. Employing higher effective shielding gas, ensuring gas tight closures, utilizing shorter and non-organic pipes.
3. Employing clean wire and substrate during fabrication.
4. Utilizing high-quality feedstock.
5. Optimizing the shape of the deposited bead.
6. Considering heat treatment as a post-processing step.

### 2.5.2 Residual stress

Residual stress is the term used to describe the internal stresses that persist within a material even after all external forces acting on it have been removed. The presence of residual stresses can significantly effect the fatigue properties and net performance of the product. When the

part is no longer held in place or supported, the presence of residual stress can result in issues such as distortion, separation between layers, compromised precision in the shape and dimensions, and a notable reduction in the ability to withstand fractures and fatigue. During fabrication, the continuous process of melting and cooling leads to thermal shrinkage and expansion, causing distortion in the part. This effect is especially prominent in large thin-walled components, where the stresses and deformation can be significant. Moreover, the stresses are most notable in the direction of deposition.

### **2.5.3 Solidification cracking**

In WAAM, it is essential to carefully select and design a fixture as it directly affects crack propagation during the final stage of solidification. The use of restraints during this stage has a crucial impact on the occurrence of crack formation. Cracking, a visible defect commonly observed in the solidification process of aluminum components during WAAM, is mainly attributed to the broad temperature range required for solidification in aluminum alloys. To mitigate the risk of solidification cracking, preheating and/or post-heat treatment methods can be employed. These measures help reduce the likelihood of crack formation.

Figure 7 shows Scanning-Electron Microscope (SEM) images illustrating the fractured surface morphology observed of WAAM of Al 2219 alloy during horizontal tensile tests conducted under different conditions. On the fractured surfaces, the appearance of dimples indicates a fracture of a ductile metal behavior. The dimension of the dimples varies among specimens subjected to different processing conditions.

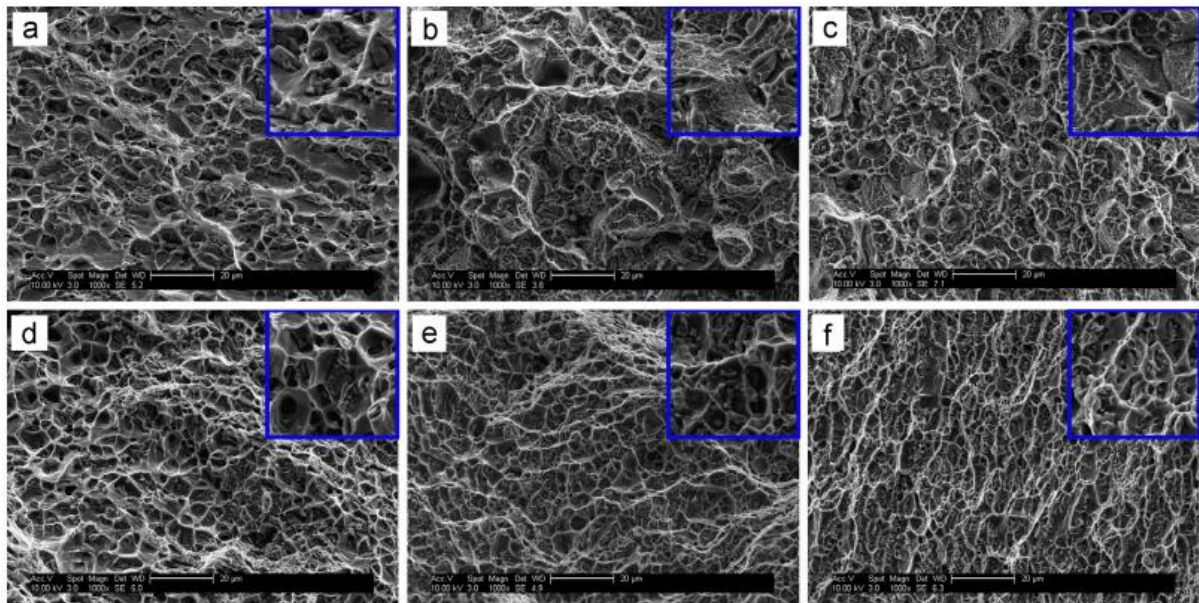


Figure 2.4. The Scanning Electron Microscope (SEM) images shows morphology of tensile metal made from WAAM Al 2219 alloy is depicted in the following conditions: (a) as-deposited metal, (b) T6 treated part, (c) 45k-N rolled followed by T6 treatment, and (d-f) 15 k-N, 30 k-N, and 45 k-N rolled part

#### 2.5.4 Fabrication set-up

Automation plays a vital role in extending the capabilities of WAAM technology, but it also poses significant challenges when it comes to practical implementation. The full potential of WAAM technology, which involves additive fabrication of components to achieve near net shape, cannot be realized without automation. To ensure efficient component production in WAAM, the utilization of automation resources is crucial. These resources consist of a CNC robotic system featuring a power source, a welding torch connected to a wire feed setup, and an online control setup. These automation tools play a vital role in recording and regulating key parameters, thereby facilitating the effective execution of the WAAM process.

#### 2.5.5 Anisotropy

The characteristics of WAAM products vary depending on the direction of deposition and the thickness of the material. The variation in properties observed in additive manufacturing is mainly attributed to the layer deposition approach. It is observed that the hardness in the final product is directly influenced by the number of layers. Specifically, the layers closer to the

component's surface undergo fewer thermal cycles, resulting in an improvement in material hardness.

### 3. METHODOLOGY

Wire-Arc additive manufacturing (WAAM) is an approach used for the layer-by-layer deposition of metal. In this process, a welding machine with a wire feed system is employed to melt and deposit metal wire onto a substrate. The metal wire is carefully selected based on the desired properties and application requirements. Process parameters and control play a vital role in achieving successful additive manufacturing. Parameters such as wire feed speed, arc voltage, current, and travel speed are set based on the specific requirements of the wire and workpiece materials. Optimal parameters are determined through experimentation and analysis. Additionally, a suitable shielding gas is employed to protect the molten pool from atmospheric contamination. The workpiece surface is prepared, and the metal wire is fed into the arc to create a molten pool. With precise control of parameters such as wire feed speed, arc voltage, current, and travel speed, the metal is deposited layer by layer, following a predetermined path. The deposited layers gradually build up to form the desired shape and geometry.

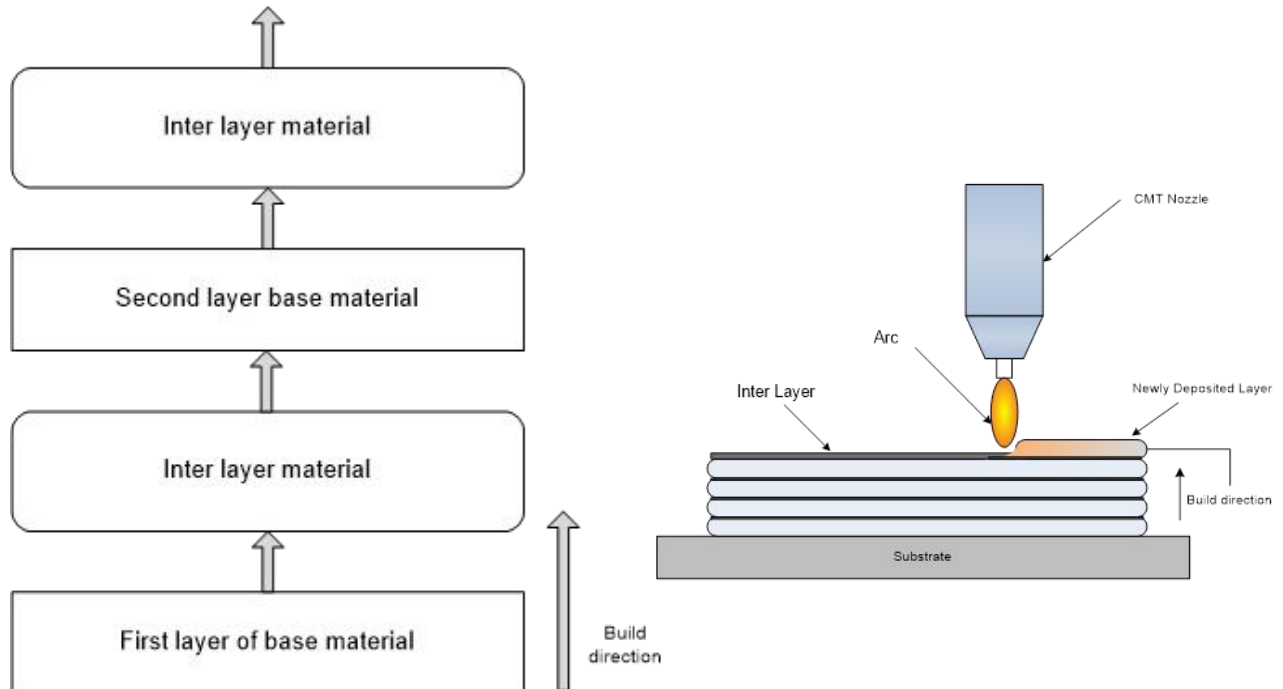


Figure 3.1. Methodology to perform WAAM

Post-processing operations such as machining and surface finishing may be performed to achieve the desired surface quality and dimensional accuracy. The methodology for wire arc additive manufacturing in a layer-by-layer fashion enables the fabrication of complex metal parts with high precision and control over the deposition process.

#### 4. EXPERIMENTAL DETAILS

Gas-metal Arc welding(GMAW) was used to perform Wire-Arc Additive Manufacturing. ER70S-6 Mild Steel wire was taken as feed wire having 1.2 mm diameter. Interlayer was distinguished with 304 Grade Stainless Steel, which was used in form of foil of 0.3 mm thickness. Wire-Arc Additive Manufacturing specimen was fabricated using Mild Steel as base material and Stainless Steel as interlayer. The interlayer Stainless Steel foil was putted after a rest of one minute. The specimen was a cuboidal wall structure with a size of 12.7 cm  $\times$  0.6 cm  $\times$  10.1 cm. Specimen top surface was polished with emery paper ranging from 200 to 2000 grit size, followed by Diamond polishing. The characterization studies done for the specimen were Optical Microscopy (OM), Energy-dispersive X-ray spectroscopy (EDS), X-ray diffraction (XRD), Scanning Electron Microscopy (SEM).



Figure 4.1. WAAM specimen fabrication method



Figure 4.2. WAAM fabricated specimen

Welding parameters that were taken while preparation of the WAAM specimen were given in Table 4.1 Wire-Arc Additive Manufacturing operation was performed using a specially



designed CNC machine Yaskawa Japan made. To produce the layered structure, weld beads were created in a closed course, beginning and finishing at the same spot, using a torch. This manufacturing technique was used to guarantee that the temperature distribution was consistent throughout each portion of the weld bead on the created layer. Furthermore, having the beginning and finish at the same position helps to stabilise the layer's overall shape. During the manufacturing of each layer, the one before it was cooled to temperatures ranging from 80°C to 100°C. As a consequence, a structure consisting of 49 levels was created.

Parameter	Value
Arc Current	225 A
Volatge	15-18 V
Wire feed rate	4 m/min
Travel speed	0.15 m/min
Shielding gas	86% Ar + 12% C + 2% O

Table 4.1. Parameters used in specimen fabrication

Microstructure characterization studies were performed by cutting out a sample from the specimen along the build-direction. The conventional techniques for preparing metallographic specimens were utilized, and the samples were treated with a nitric acid

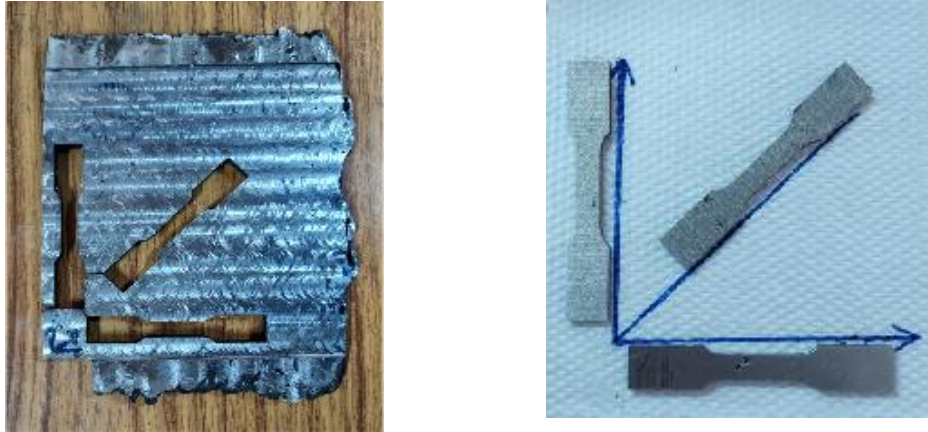


Figure 4.3. Section of specimen cut from sample

solution containing 2% concentration for etching. To analyze the phase structure of the



WAAM specimen, the XRD (X-ray diffraction) test was conducted on the sample taken from specimen. Two specimen were prepared, first having only ER70S-6 Mild steel, and the other having 304 Stainless Steel as intelayer metal. Additionally, hardness measurements was performed at top and bottom face of the sample of specimen, which had been prepared for



microstructure analysis. For each measurement three trails were

Figure 4.4. Samples taken from WAAM using EDM

done. In Fig 4.3 red dotted rectangular box shows the section of the specimen from where the sample is cut using Electro-discharge machining. Hardness measurement was done using Vickers micro-hardness test. A load of 300 grams was applied for a dwell time of 10 seconds. WAAM specimen was milled to get a specimen to perform tensile test.

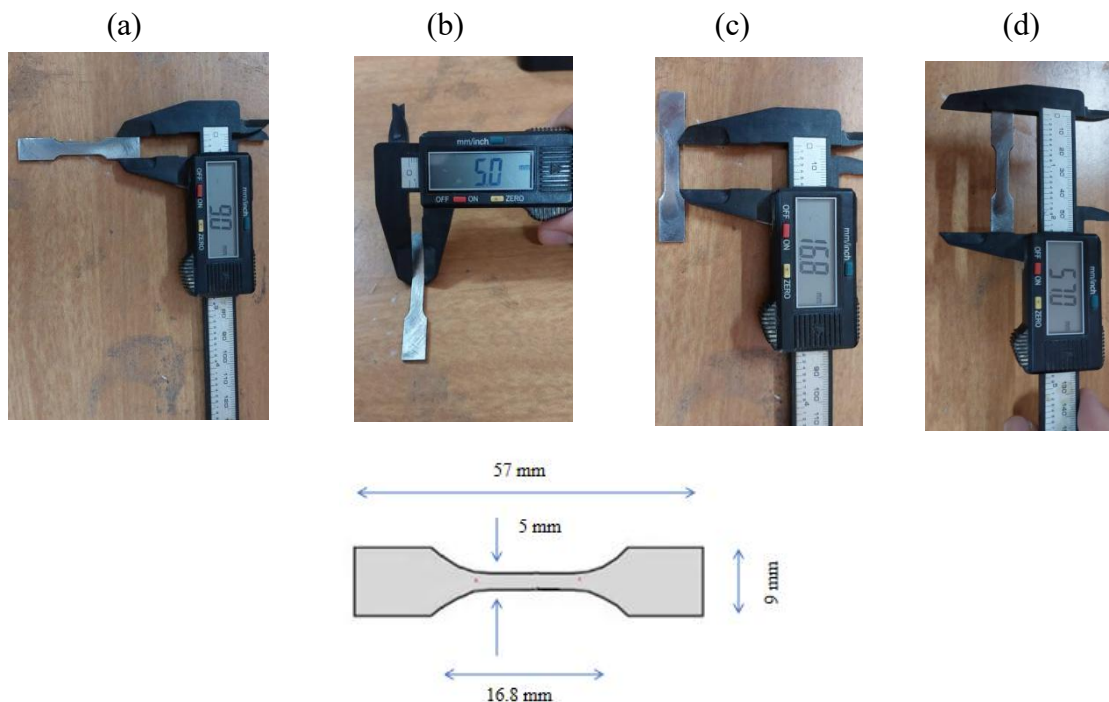


Figure 4.5. Dog bone specimen for tensile test with dimensions (a) 9.00 mm breadth, (b) 5.00 mm guage breadth, (c) 16.80 mm guage length, (d) 57.00 mm length of specimen

The specimen was machined in equal amounts from both WAAM surfaces to produce a wall like structure of approximately 6 mm thickness. Specimens were then cut using wire Electric-discharge machining (EDM) method. Fig 4.4 shows the section from which the samples were cut for performing tensile test. The samples were taken along horizontal, vertical and diagonal directions to do tensile test, and a comparison was drawn between them. The dimensions of tensile test specimen are shown in Fig 4.5. The test was conducted according to the ASTM E8 standard.

## 5. RESULTS

The sample taken from specimen having 304 Stainless steel interlayer had a mass of 6.2585 grams, and the sample taken from specimen without any interlayer (that is only ER70S-6 Mild Steel) had a mass of 6.2058 grams. The two samples were compared for their mechanical properties to judge the effect of adding interlayer on the Hardness and Strength of the alloy. Table 5.1 shows the density and mass of the samples acquired from the two specimens. The specimen without interlayer prepared using layer by layer deposition of ER70S-6 consists of C 0.08%, Si 0.93%, Mn 1.38% , Fe 96.61% and other minor elements.

Sample	Mass (grams)	Density (Kg/m <sup>3</sup> )
Sample with 304 Stainless Steel interlayer	6.2585	7699.85
Sample without interlayer	6.2058	7471.6

Table 5.1. Density and mass of the samples

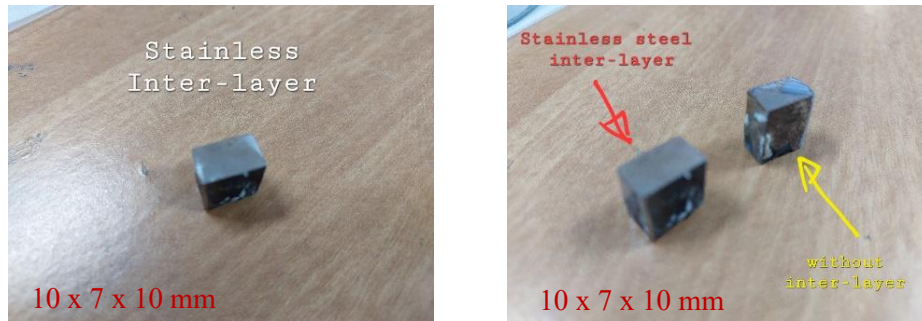


Figure 5.1. WAAM Mild Steel with and without interlayer Specimen

The specimen with interlayer prepared using 304 Stainless Steel sandwiched between ER70S-6 Mild Steel consists of C 0.12%, Si 0.67%, Cr 0.02%, Mn 0.98%, Ni 2.29%, Fe 94.31% and other minor elements. Electric-discharge spectroscopy was used to analyze the composition of the specimen. The results of the test are shown in Fig 5.2 and Fig 5.3

### 5.1 Micro-structure characterization

#### 5.1.1 Energy-dispersive X-ray spectroscopy (EDS)

Also referred to as EDX, EDXS, XEDS, EDXA, or EDAX, is an analytical technique utilized for the elemental analysis and chemical characterization of a given sample. This method relies on the interaction between the sample and an X-ray excitation source. The capacity of EDS to characterize materials stems from the fundamental concept that each element possesses a unique atomic structure, resulting in a distinct set of peaks on its electromagnetic emission spectrum, as observed in spectroscopy.

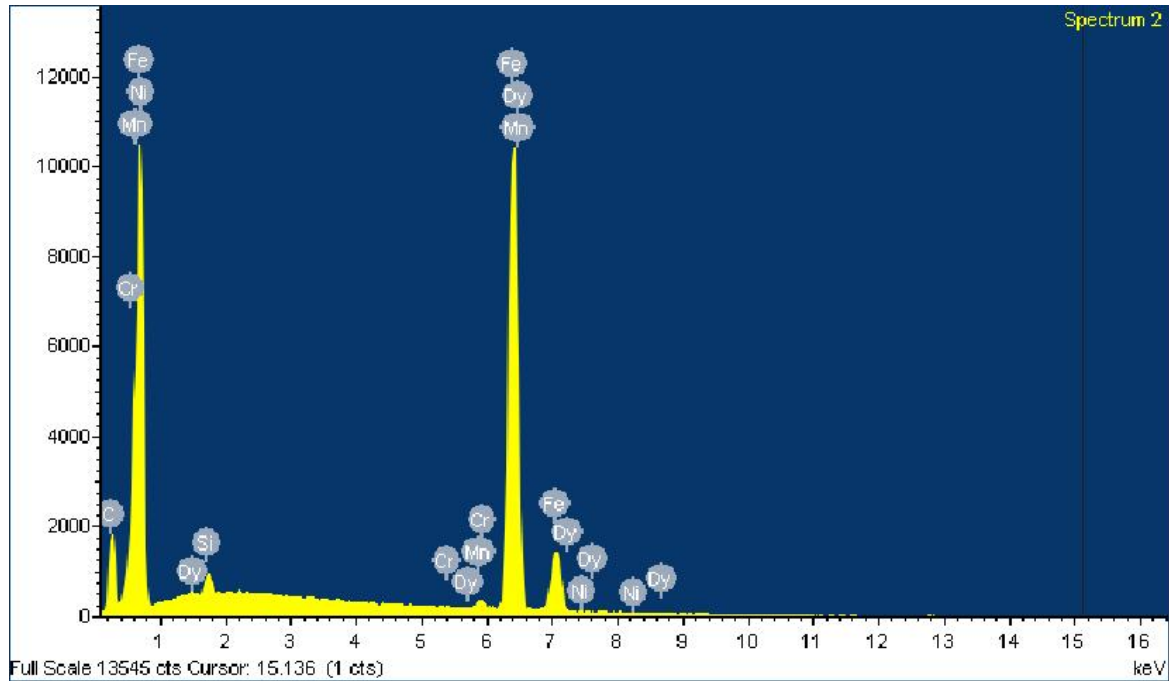


Figure 5.2. EDS Characterization to see the composition of WAAM specimen

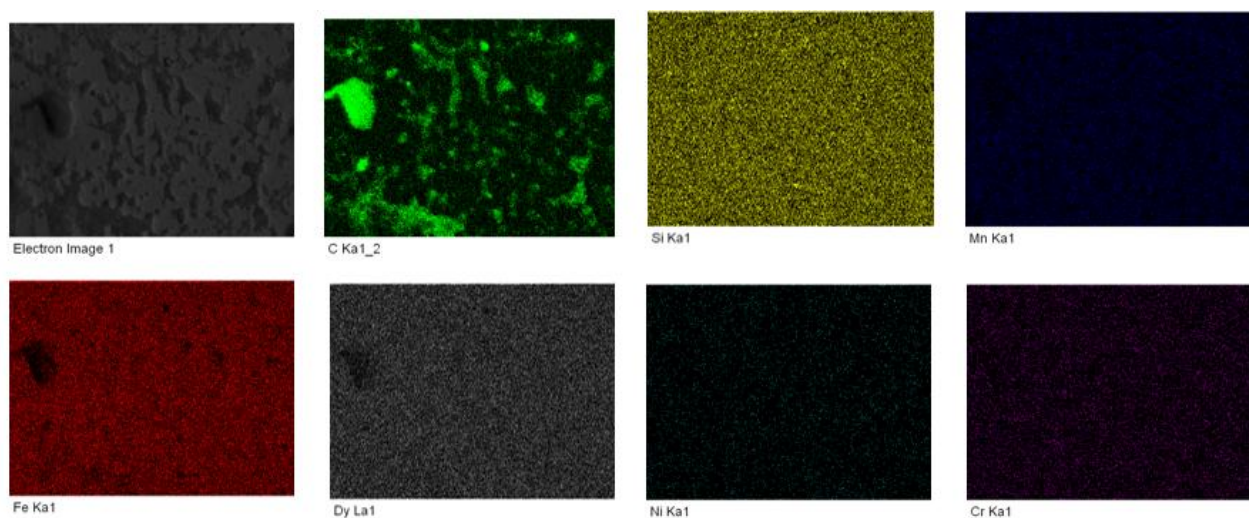


Figure 5.3. Dispersion of elements in specimen (a) Electron image, (b) Carbon (green), (c) Silicon (golden), (d) Manganese (blue), (e) Iron (red), (f) Dysprosium (grey), (g) Nickel (cyan), (h) Chromium (violet)

The accuracy of peak positions in EDS is greatly predicted by Moseley's law, surpassing the experimental resolution of a typical EDX instrument. To initiate the emission of identifiable X-rays from the specimen, a focused electron beam is directed onto the specimen under examination. In the sample, an atom's ground state electrons, also known as unexcited electrons, are confined to specific energy levels or electron shells while in a resting state. When the incident beam excites an electron in an inner shell, it is dislodged from its shell, leaving behind an electron hole. The energy disparity between the higher-energy outer shell and the lower-energy inner shell is then released in the form of an X-ray as an electron from the outer, higher-energy shell fills the vacancy created by the ejected electron. By employing an energy-dispersive spectrometer, the quantity and energy of the X-rays emitted from the specimen can be determined. The result of EDS characterization for the specimen having 304 Stainless Steel interlayer between ER70S-6 Mild Steel is shown in Table 5.2.

Element	Weight %	Atomic %
C K	0.12	1.02
Si K	0.67	0.97
Cr K	0.02	0.02
Mn K	0.98	0.73
Fe K	95.83	95.17
Ni K	2.29	1.58
Dy L	0.08	0.51

Table 5.2. Composition of WAAM specimen with SS interlayer

### 5.1.2 Optical Microscopy (OM)

The optical microscope utilizes visible light and a series of lenses to produce enlarged images of small objects. The Olympus inverted optical microscope is employed to examine the morphology of specimens. To observe the sample, it is placed on a platform and viewed closely through one or both eyepieces of the microscope. In high-power microscopes, both eyepieces typically present the same image, while a stereo microscope creates a three-dimensional effect by using slightly different images. The captured image is usually recorded using a camera, resulting in a micrograph. The characteristics and size of the diffraction patterns are influenced by factors such as the wavelength of light ( $\lambda$ ), the refractive materials utilized in the production of the objective lens, and the numerical aperture (NA) of the



objective lens. The microstructure of the sample having 304 Stainless steel sandwiched between ER70S-6 Mild steel is shown in Fig 5.4.

The presence of ferrite region and lamellar pearlite can be seen from the optical micrographs of the WAAM sample. White portion are ferrite grains, with green portion showing pearlite. The grain are coarse which is due to grain size being greater than  $15\text{ }\mu\text{m}$ .

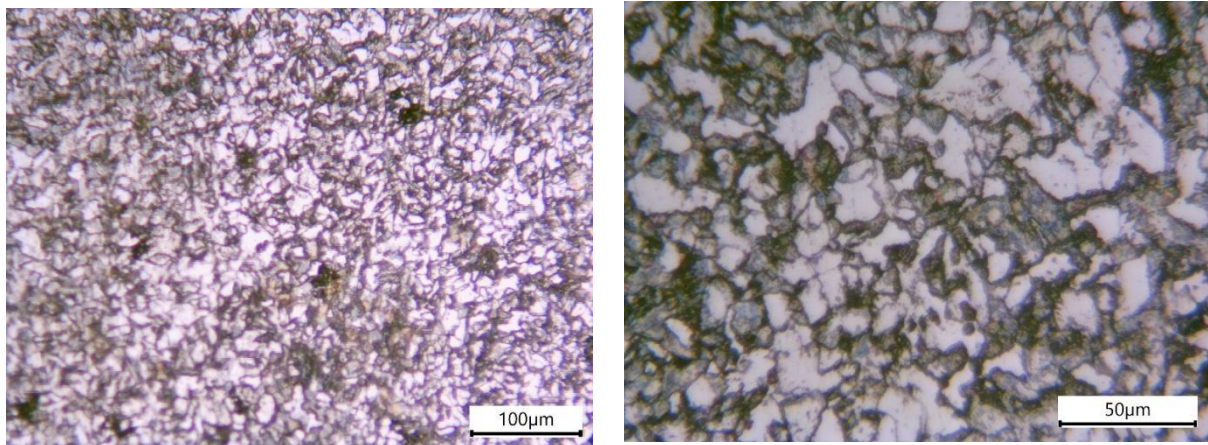


Figure 5.4. Microstructure image received from Optical Microscope, at resolution of  $100\mu\text{m}$  and  $50\mu\text{m}$

Analysis of the grain size and grain area for pearlite and ferrite grain found in optical microscopic image was performed. Average ferrite grain size was found to be  $20.9775\text{ }\mu\text{m}$ , with grain area of  $2.1389\text{ }\mu\text{m}^2$ . This is shown in Fig 5.5 (a). Average pearlite grain size was found to be  $16.6641\text{ }\mu\text{m}$ , with pearlite grain area of  $0.1434\text{ }\mu\text{m}^2$ . This can be seen in Fig 5.5 (b).

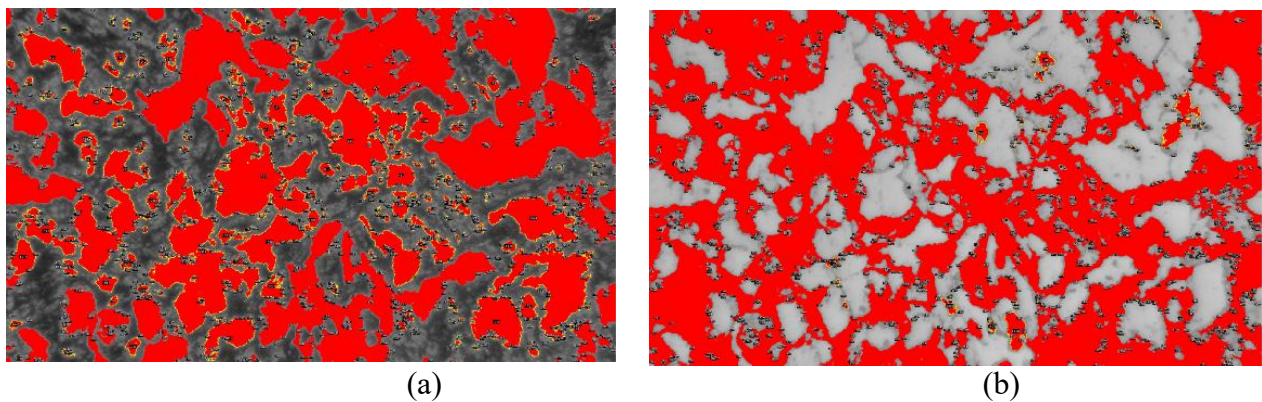
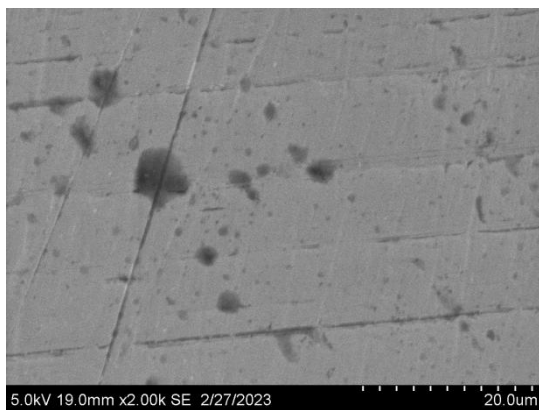


Figure 5.5. Grain size and grain area analysis of WAAM specimen with SS interlayer (a) Ferrite region, (b) Pearlite region

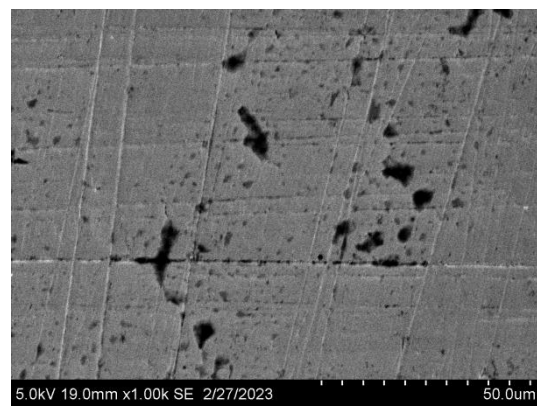
### 5.1.3 Scanning Electron Microscopy (SEM)

A scanning electron microscope (SEM) utilizes a focused electron beam to examine the surface of a sample, generating visual representations. The signals produced by the interaction between the electrons and the atoms on the sample's surface unveil its topographical features and chemical composition. To construct an image, the electron beam's position is combined with the strength of the detected signal while scanning in a predetermined pattern. In the widely used mode of SEM, a secondary electron detector called the Everhart-Thornley detector is employed to locate secondary electrons released by excited atoms. The amount of secondary electrons that can be detected, and therefore the intensity of the signal, is influenced by the specimen's topography. A scanning electron microscope (SEM) generates images by utilizing signals produced from the interactions between the electron beam and atoms located at various depths within the sample. These interactions give rise to different types of signals, including secondary electrons (SE), reflected or backscattered electrons (BSE), characteristic X-rays and light (cathodoluminescence), absorbed current (specimen current), and transmitted electrons. While secondary electron detectors are typically included as a standard component in all SEMs, it is unusual for a single instrument to possess detectors for all potential signals.

(a)



(b)



(c)

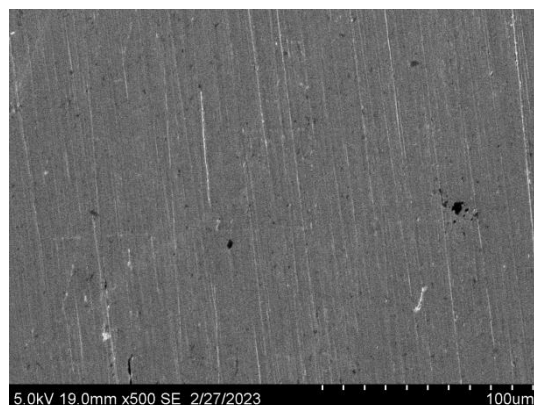


Figure 5.6. SEM images of WAAM specimen without interlayer with resolution of, (a) 20  $\mu\text{m}$ , (b) 50  $\mu\text{m}$ , (c) 100  $\mu\text{m}$

SEM images of sample without interlayer, which is only composed of ER70S-6 Mild steel can be seen in Fig 5.6. The sample with 304 Stainless steel sandwiched between ER70S-6 Mild steel as interlayer, SEM image is shown in Fig 5.7 at resolutions of 20  $\mu\text{m}$ , 50  $\mu\text{m}$  and 100  $\mu\text{m}$ . The analysis of porosity present in sample was conducted using the SEM images. Porosity is one of the major defect in WAAM, which reduces the strength of the functional part, so one of the objective of this research work is to reduce porosity presence.

The porosity present was successfully reduced by introducing an interlayer of Stainless steel. The porosity size present in WAAM sample without interlayer was 3.209  $\mu\text{m}$  in diameter, which was reduced to 0.921  $\mu\text{m}$ . The average porosity area was decreased from 14.093  $\mu\text{m}^2$  to 1.094  $\mu\text{m}^2$ .

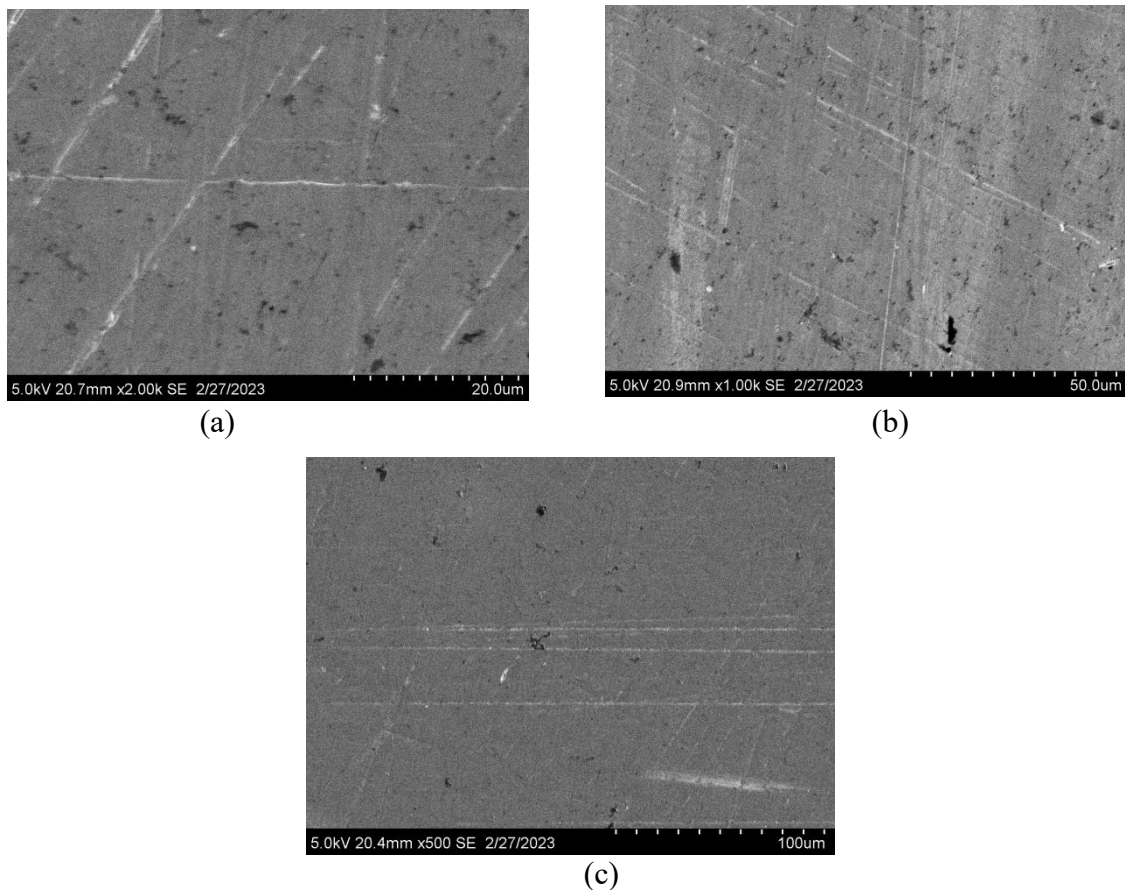


Figure 5.7. SEM images of WAAM specimen with 304 Stainless steel interlayer with resolution of, (a) 20  $\mu\text{m}$ , (b) 50  $\mu\text{m}$ , (c) 100  $\mu\text{m}$



A comparison is shown in Fig 5.8 which is used to analyse the porosity present in WAAM sample with Stainless steel interlayer and without interlayer. Table 5.3 summarizes the effect on porosity by using 304 SS interlayer between ER70S-6 Mild steel layers.

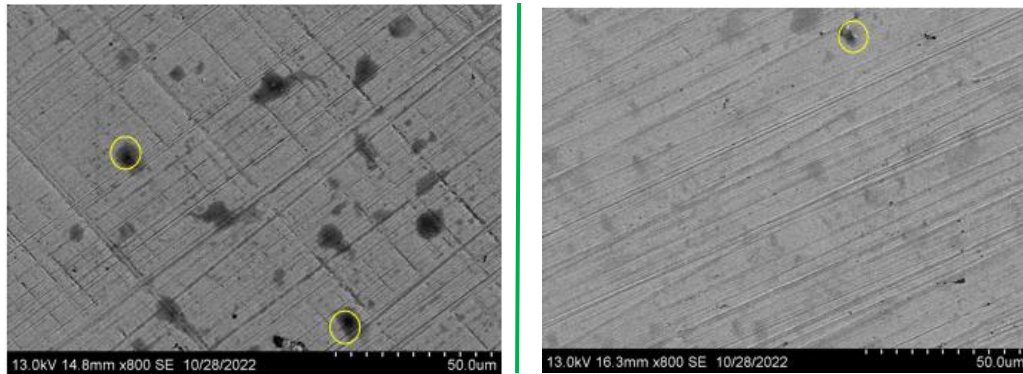


Figure 5.8. Comparison between WAAM sample with and without interlayer to analyse porosity

The percentage of porosity present in the sample was reduced to 0.0355% from 0.1843% by introducing an interlayer of 304 Stainless steel between ER70S-6 Mild steel layers.

Parameter	Without interlayer	With 304 SS interlayer
Average porosity size	3.209 $\mu\text{m}$	0.921 $\mu\text{m}$
Average porosity area	14.093 $\mu\text{m}^2$	1.094 $\mu\text{m}^2$
Porosity presence %	0.1843%	0.0355%

Table 5.3. Analysis of Porosity present in WAAM samples

#### 5.1.4 X-ray diffraction (XRD)

X-ray diffraction analysis (XRD) is a technique employed in materials science to determine the crystallographic structure of a substance. When X-rays interact with a material, XRD measures the intensities and scattering angles of the X-rays after they pass through the material. One of the primary applications of XRD analysis is the identification of materials based on their diffraction patterns. Additionally, XRD provides insights into how internal stresses and defects cause deviations from the ideal crystal structure.

X-rays, which can be considered as waves of electromagnetic radiation, interact with the orderly arrangement of atoms in crystals. Specifically, the electrons associated with the crystal atoms play a significant role in scattering the incident X-rays. This scattering process is

known as elastic scattering, where the electron acts as the scatterer. The regular arrangement of scatterers gives rise to a regular pattern of spherical waves. In most directions, these waves interfere destructively, resulting in their cancellation. However, in a few specific directions determined by Bragg's law, they exhibit constructive interference.

Bragg's law can be represented by the equation:

$$n\lambda = 2d \sin(\theta),$$

where  $d$  represents the spacing between the diffracting planes,  $\theta$  is the incident angle,  $n$  is an integer, and  $\lambda$  is the wavelength of the X-ray beam. These specific directions manifest as reflections or spots on the diffraction pattern. Consequently, X-ray diffraction patterns emerge from the interaction of electromagnetic waves with a well-ordered array of scatterers.

XRD analysis results shows that the ER70S-6 Mild steel specimen with 304 Stainless steel interlayer has BCC  $\alpha$ -ferrite phase as main constituent. The peaks in XRD result are found at the  $2\theta$  angles of  $44.833^\circ$ ,  $65.186^\circ$  and  $82.352^\circ$ . The  $h, k, l$  planes corresponding to the peaks are (1 1 0), (2 0 0), and (2 1 1) respectively. Presence of pearlite phase, along with ferrite was also evident from the XRD analysis. The lattice structure was found to be Cubic.

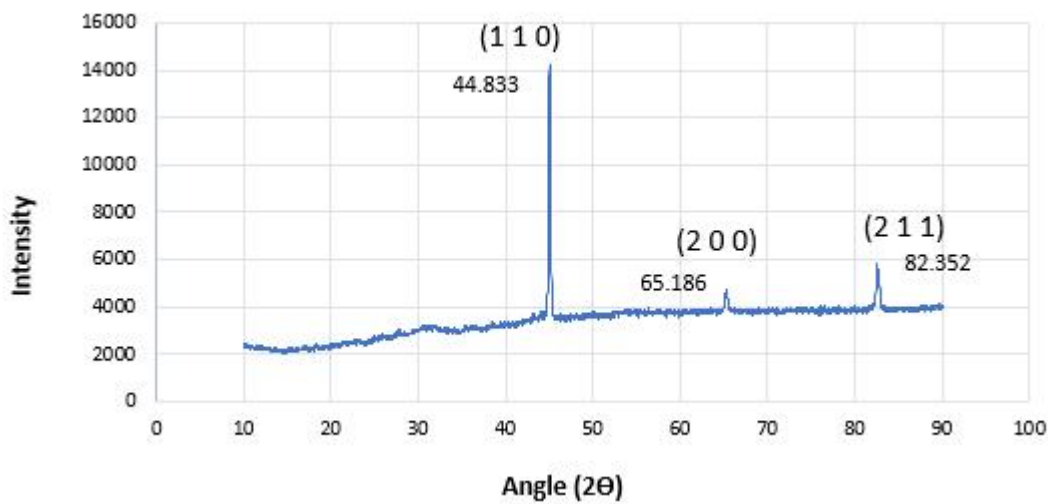


Figure 5.9. Plot of data received from XRD

The results of XRD is shown in Table 5.4, the peak angles and corresponding planes can be seen. The Inter-planar distance ( $d$ ) is also mentioned. For the plane (1 1 0) the inter-planar distance was  $2.02 \times 10^{-10}$  m, for the plane (2 0 0) inter-planar distance was  $1.43 \times 10^{-10}$  m, and for the plane (2 1 1) the inter-planar distance was found to be  $1.17 \times 10^{-10}$  m.

Peak no.	2 $\theta$ (degree)	h	k	l	d ( x 10 <sup>-10</sup> m )
1	44.833	1	1	0	2.02
2	65.186	2	0	0	1.43
3	82.352	2	1	1	1.17

Table 5.4. Planes corresponding to peaks of XRD

## 5.2 Mechanical Tests

### 5.2.1 Tensile testing

The tensile test is used to evaluate the mechanical properties, specifically the strength and ductility, of metallic materials. It involves subjecting a standardized metal specimen to an axial force, incrementally applying tension until the specimen fractures. This test enables the determination of critical parameters such as yield strength, ultimate tensile strength, elongation, and reduction in area. During the tensile test, the standardized specimen is securely clamped at its ends and subjected to a progressively increasing load. As the load is applied, the specimen undergoes deformation, experiencing elongation along the axial direction. The relationship between the applied force and the resulting elongation is precisely measured, facilitating the construction of a stress-strain curve. The stress-strain curve derived from the tensile test provides valuable insights into the mechanical behavior of the material. Initially, the material undergoes elastic deformation, displaying a linear stress-strain relationship within the elastic range. This linear relationship is quantified by the elastic modulus, commonly referred to as Young's modulus. Upon surpassing the elastic limit, the material enters the region of plastic deformation, resulting in permanent elongation. The stress required to induce this permanent deformation is denoted as the yield strength. Beyond the yield point, the material exhibits strain hardening, which necessitates an increased stress magnitude to induce further plastic deformation. The ultimate tensile strength denotes the maximum stress that the material can sustain before fracturing. At this critical point, the material initiates necking, wherein a localized reduction in the cross-sectional area occurs. The extent of necking and the subsequent reduction in area provide significant insights into the material's ductility properties.

Tensile test was performed along three directions- horizontal, vertical and diagonal of the specimen. Wire EDM was used to cut the samples along the three directions. The tests were

performed on a Universal Testing Machine of 500 kN load capacity, with Strain rate of 1 mm/min. The specimen was prepared according to ASTM E8 standards, with the nominal dimensions of 16.8 x 5 mm. The Ultimate tensile strength for specimen cut along horizontal was found to be 508.3756 MPa, in vertical direction it was 500.4092 MPa, and in diagonal direction it was 491.0566 MPa.

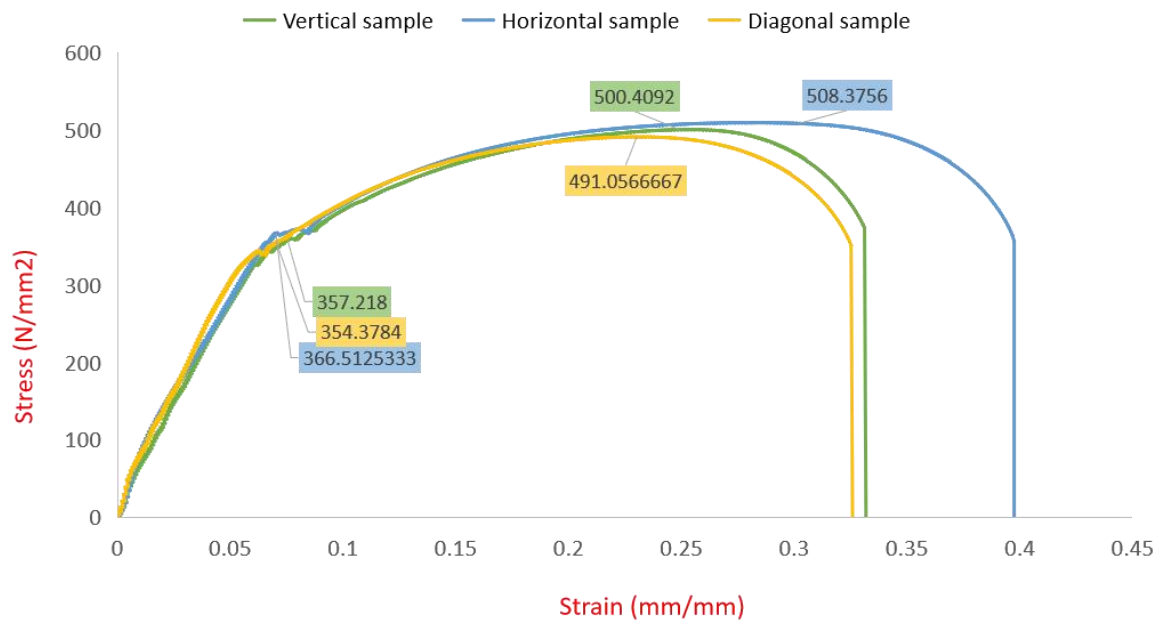


Figure 5.10. Tensile test result for WAAM specimen with SS interlayer along horizontal, vertical, and diagonal directions.

The tensile specimen broke with a cup and cone fracture, which can be observed from Fig 5.11 (b). This type of fracture is particular to metals subjected to uni-directional load. The Ultimate strength along the horizontal direction, is cause of less number of interlayers along this direction, compared to vertical and diagonal direction.

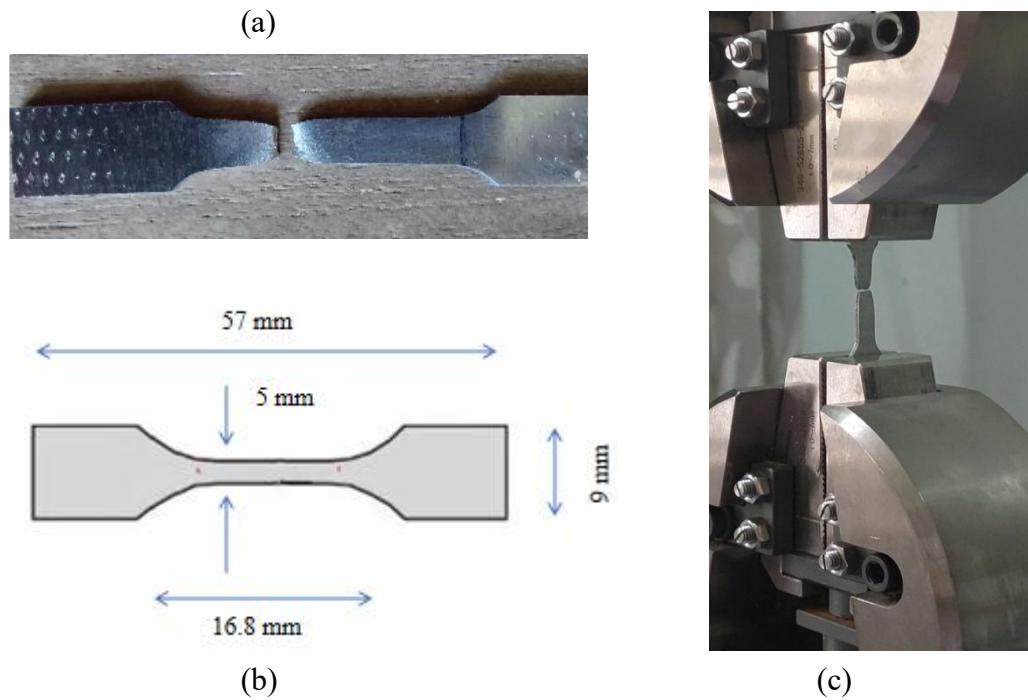


Figure 5.11. Tensile test specimen (a) dimensions of the specimen, (b) fractured specimen with cup and cone fracture, (c) specimen under load in UTM

The specimen with Stainless steel interlayer and the specimen without interlayer were having similar tensile strength. WAAM specimen without interlayer was more ductile and tough than the specimen with Stainless steel interlayer, which is evident from the graph plotted between the two specimens, shown in Fig 5.12. This can be due to the low carbon percentage present in specimen made only with ER70S-6 Mild steel without any interlayer alloy.

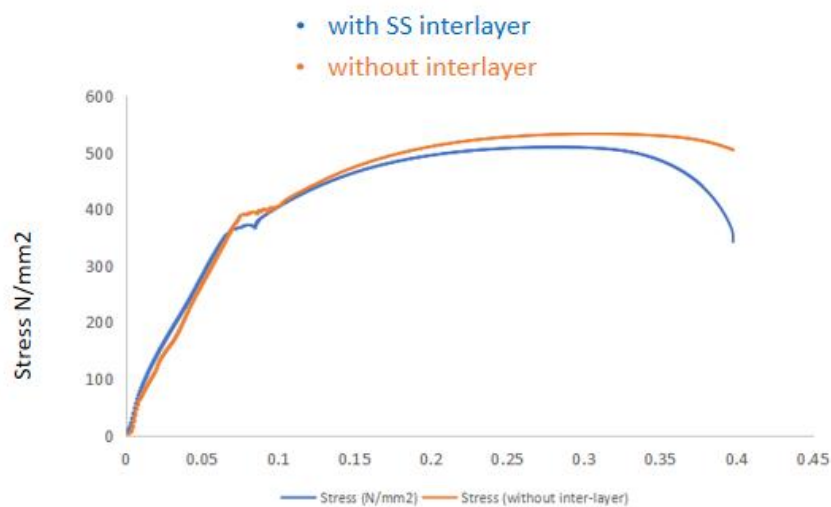


Figure 5.12. Comparison of WAAM specimen with and without interlayer

### 5.2.2 Micro-hardness testing

The Vickers microhardness test is a technique for assessing the hardness of materials at small scales. It entails exerting a predetermined force onto the surface of a specimen using a diamond indenter with a pyramid shape. The indenter produces an impression on the material, and the dimensions of the impression are quantified to determine the material's hardness. To perform the test, the specimen is securely affixed to a microscope stage, and the indenter is pressed into the material with a precise load. The load typically falls within the range of a few grams to several kilograms, and it is sustained for a specific period, usually between 10 to 15 seconds. Following the release of the load, the resulting indentation is measured using either an optical microscope or an automated measurement system. The Vickers indenter possesses a square-based pyramid configuration with an included angle of 136 degrees between opposite faces. This geometric design facilitates accurate and replicable indentations on a diverse array of materials, encompassing metals, ceramics, and composites. The size of the indentation, commonly expressed as the diagonal length of the impression, directly correlates with the material's hardness. The Vickers microhardness test confers several advantages. It enables hardness evaluations on diminutive or thin samples, coatings, or specific regions of a material. It delivers precise and dependable hardness measurements, and the test outcomes can be utilized for material comparisons, characterization of material properties, or assessment of the impact of treatments or processes on the material's hardness.

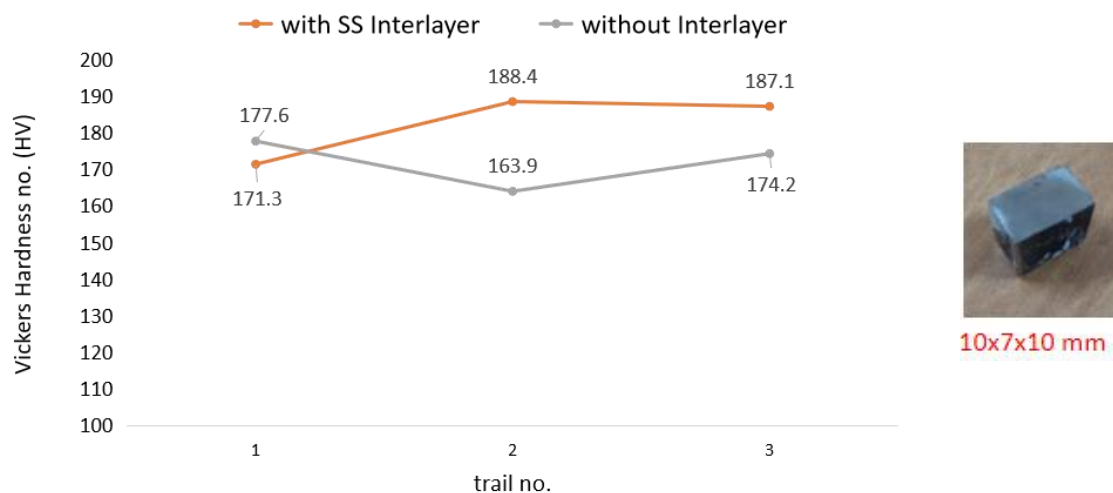


Figure 5.13. Vickers microhardness test for the WAAM specimen with SS interlayer and without interlayer

Hardness test was conducted by applying a load of 300 grams on the sample for a dwell time of 10 seconds. Three trials were performed for both the sample, with 304 Stainless steel interlayer and without interlayer. The Fig 5.13 shows, the sample with Stainless steel interlayer between ER70S-6 Mild steel layers had more hardness in comparison to the sample made only with ER70S-6 Mild steel. The greater hardness of sample with Stainless steel is due the presence of Chromium in specimen. The hardness value for the three trials on the specimen with Stainless steel interlayer were 171.3 HV, 188.4 HV and 187.1 HV. The harness value for the specimen without interlayer were 177.6 HV, 163.9 HV and 174.2 HV.

## 6. CONCLUSION

The main steps of WAAM process planning are the optimization of welding parameters and the selection of the optimal tool path. WAAM's potential new developments include porosity control, residual stresses, and high heat input. Because the fabrication quality and material properties govern the fundamental affinity between composition and microstructure of material, it is crucial to match the WAAM process performance features with the understanding of material characteristics in order to fabricate high-quality and defect-free components. As we have discussed in the methodology section that as each layer goes through the cycle of heating and cooling and therefore its microstructure changes and is different to its previous layers. For manufacturing of the taller structures some more ways and processes can be made to make the product more homogenous in microstructure. The main inferences from the research work can be concluded as

- The Average grain size for Ferrite and Pearlite is greater than  $15\mu\text{m}$ , thus giving coarse grain structure
- Peak planes are (110), (200), and (211) at  $44.833^\circ$ ,  $65.186^\circ$ ,  $82.352^\circ$  respectively which, corresponds to Ferrite
- The specimen with Stainless Steel interlayer is composed of Ferrite, with BCC lattice, and lamellar pearlite
- Comparing to specimen without SS interlayer, the specimen with SS has more Ferrite phase
- Porosity is decreased on adding the SS interlayer, from 0.1843% to 0.0355% Area density
- Hardness of sample with SS interlayer is greater than without interlayer due to presence of Cr, causing Solid Solution hardening
- Average Hardness of the Stainless Steel interlayered WAAM Specimen is 182.26 HV
- The Ultimate tensile strength and Yield strength of vertical, horizontal and diagonal samples are approximately similar:- thus Isotropic property



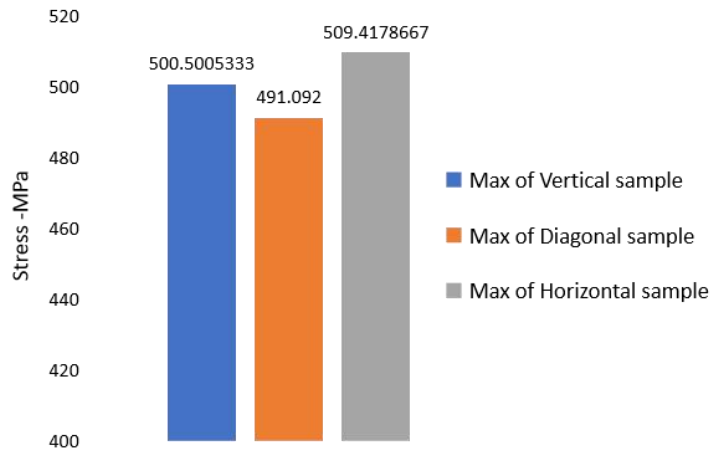


Figure 6.1. Comparison of Ultimate tensile of the WAAM specimen along three directions

- Ductility variation in horizontal sample and vertical, diagonal sample can be due to-
  - i. Presence of porosity or manufacturing discontinuity
  - ii. Presence of coarse grains along HAZ

However, out of all metal deposition AM techniques, WAAM appears to be the most qualified candidate to replace the current processes of producing parts from forgings or billets, particularly for the aerospace industry. Instead of focusing on a single system to solve all of the potential issues and challenges faced by the industrial community, WAAM techniques should be well optimized for a specific area application. Further study in WAAM could transform it from a near net shaping process to a net shaping process for better industry adoption.

## **7. FUTURE WORK**

WAAM is the future of the industry as it provides low cost and high deposition rate. But for WAAM to become more feasible the researchers need to work on some of its limitations. This section provides some problems that if we solve can make WAAM more useful than ever. In future the WAAM can make use of multi-material wires and make complex structure which are difficult to make even with the conventional techniques. although there are many defects regarding multi material WAAM. In future, work can be done to minimize multi-material defects.

Many WAAM finished products require additional post processing treatment like heat treatment, rolling and plastic deformation to get to the strength as of the same product produced from the conventional way. In future the work can be done to reduce the post processing to the minimum so that it will take less time for production. In future the work can be done to produce more functional products rather than simple geometric shapes. So that it can be reached in commercial market also. And also since we are testing on the standard shapes, we have very little idea of how the product will perform in the application so more test can be made to test the performance of the product in respective applications. Mechanical Properties testing to analyse the effect of inter-layer on base Material can be done. Study the effects of varying machine parameters, like Wire feed rate, Arc Current could be performed in future.

## 8. REFERENCES

- [1]. A. Su, S.J. Al'Aref, in: 3D Printing Applications in Cardiovascular Medicine, Elsevier, 2018, pp. 1-10.
- [2]. T. Sathish, K. Muthukumar, B. Palani Kumar, *Int. J. Mech. Prod. Eng. Res. Develop.* 8 (2018) 1515–1535.
- [3]. T. Sathish, J. Jayaprakash, *Int. J. Logist. Syst. Manage.* 26 (2017) 402–419.
- [4]. T. Sathish, A. Muthulakshmanan, *J. Appl. Fluid Mech.* 11 (2018) 39–44.
- [5]. T. Sathish, P. Periyasamy, D. Chandramohan, N. Nagabhooshanam, *Int. J. Mech. Prod. Eng. Res. Develop.* (2018) 711–716.
- [6]. T. Sathish, *Mater. Today.: Proc.* 5 (2018) 14416–14422.
- [7]. D. Madan, C. Sivakandhan, S. Sagadevan, T. Sathish, *Int. J. Mech. Prod. Eng. Res. Develop.* (2018) 582–590.
- [8]. T. Sathish, M.D. Vijayakumar, A. Krishnan Ayyangar, *Mater. Today: Proc.* 5 (2018) 14489–14498.
- [9]. T. Sathish, P. Periyasamy, D. Chandramohan, N. Nagabhooshanam, *Int. J. Mech. Prod. Eng. Res. Develop.* (2018) 705–710.
- [10]. I. Gibson, D. Rosen, B. Stucker, *Additive Manufacturing Technologies*, Springer New York, New York, NY, 2015, <https://doi.org/10.1007/978-1-4939-2113-3>.
- [11]. Panchenko, O.V.; Zhabrev, L.A.; Kurushkin, D.V.; Popovich, A.A. Macrostructure and Mechanical Properties of Al – Si, Al – Mg – Si, and Al – Mg – Mn Aluminum Alloys Produced by Electric Arc Additive Growth. *Met. Sci. Heat Treat.* 2019, 60, 749–754.
- [12]. B. Ralph, Method of making decorative articles. United States, US1533300A. Filed Nov. 12, 1920, Granted April 14, 1925., n.d.
- [13]. Mohebbi, M.S.; Kühl, M.; Ploshikhin, V. A thermo-capillary-gravity model for geometrical analysis of single-bead wire and arc additive manufacturing (WAAM). *Int. J. Adv. Manuf. Technol.* 2020, 109, 877–891.
- [14]. T. Sathish, *Prog. Ind. Ecol.* 12 (2018) 112–119.
- [15]. J. Wang, Z. Pan, Y. Ma, Y. Lu, C. Shen, D. Cuiuri, H. Li, *Mater. Sci. Eng.: A* 734 (2018) 110–119.
- [16]. Feldmann, M.; Kühne, R.; Citarelli, S.; Reisgen, U.; Sharma, R.; Oster, L. 3D-Drucken im Stahlbau mit dem automatisierten Wire Arc Additive Manufacturing. *Stahlbau* 2019, 88, 203–213.

- [17]. Fastech.com. “Aerospace Manufacturing”; <https://www.aero-mag.com/harlow-fastech-metal-additive-manufacturing-02122020>, 2020.
- [18]. Additive manufacturing. com. Hidden complexities of wire arc additive manufacturing”; 2020. <https://www.additivemanufacturingmedia/articles/the-hidden-complexities-of-wire-arc-additive-manufacturing>.
- [19]. Gardner, L.; Kyvelou, P.; Herbert, G.; Buchanan, C. Testing and initial verification of the world’s first metal 3D printed bridge. *J.Constr. Steel Res.* 2020, 172, 106233.
- [20]. Josten, A.; Höfemann, M. Arc-welding based additive manufacturing for body reinforcement in automotive engineering. *Weld. World* 2020, 64, 1449–1458.
- [21]. van Le, T.; Paris, H. On the use of gas-metal-arc-welding additive manufacturing for repurposing of low-carbon steel components: Microstructures and mechanical properties. *Weld. World* 2020.
- [22]. Wu, R.; Yu, Z.; Ding, D.; Lu, Q.; Pan, Z.; Li, H. OICP: An Online Fast Registration Algorithm Based on Rigid Translation Applied to Wire Arc Additive Manufacturing of Mold Repair. *Materials* 2021, 14, 1563.
- [23]. Li, X.; Han, Q.; Zhang, G. Large-size sprocket repairing based on robotic GMAW additive manufacturing. *Weld. World* 2021.
- [24] B. Ralph, Method of making decorative articles. United States, US1533300A. Filed Nov. 12, 1920, Granted April 14, 1925.
- [25] Williams SW, Martina F, Addison AC, Ding J, Pardal G, Colegrove P. Wire + Arc additive manufacturing. *Materials Science and Technology* 2016;32(7):641–7.
- [26] Phillips D.H. 2.1 Fundamentals and Principles of Arc Welding, in *Welding Engineering - An Introduction*, Joh Wiley & Sons, 2016.
- [27] Sequeira Almeida PM, Williams SW. Innovative process model of Ti-6Al-4V additive layer manufacturing using cold metal transfer (CMT), *Proceedings of the 21st Annual International Solid Freeform Fabrication Symposium* Austin, 2010.
- [28] Pickin CG, Young K. Evaluation of cold metal transfer (CMT) process for welding aluminium alloy. *Science and Technology of Welding and Joining* 2006;11(5): 583–5.
- [29] Lorenzin G, Rutili G. The innovative use of low heat input in welding: experiences on “cladding” and brazing using the CMT process. *Welding International* 2009;23 (8):622–32.
- [30] Martina F, Mehnen J, Williams SW, Colegrove P, Wang F. Investigation of the benefits of plasma deposition for the additive layer manufacture of Ti-6Al-4V. *Journal of Materials Processing Technology* 2012;212(6):1377–86.

- [31] Abe T, Sasahara H. Layer geometry control for the fabrication of lattice structures by wire and arc additive manufacturing. *Additive Manufacturing* Aug. 2019;28: 639–48.
- [32] Xia C, et al. Model predictive control of layer width in wire arc additive manufacturing. *Journal of Manufacturing Processes* 2020;58:179–86.
- [33] Laghi V, Palermo M, Gasparini G, Girelli V, Trombetti T. On the influence of the geometrical irregularities in the mechanical response of Wire-and-Arc Additively Manufactured planar elements. *Journal of Constructional Steel Research* 2021; 178:106490.
- [34] Kyvelou P, Huang C, Gardner L, Buchanan C. Structural testing and design of wire arc additively manufactured square hollow sections. *Journal of Structural Engineering* 2021;147(12):04021218.
- [35] Gardner L, Kyvelou P, Herbert G, Buchanan C. Testing and initial verification of the world's first metal 3D printed bridge. *Journal of Constructional Steel Research* 2020;172:106233.
- [36] Cunningham CR, Wang J, Dhokia V, Shrokani A, Newman ST. Characterisation of austenitic 316LSi stainless steel produced by wire arc additively manufacturing with interlayer cooling. *Solid Freeform Fabrication Symposium Conference* 2019. USA: Austin, Texas; 2019.
- [37] Xu F, et al. Realisation of a multi-sensor framework for process monitoring of the wire arc additive manufacturing in producing Ti-6Al-4V parts. *International Journal of Computer Integrated Manufacturing* 2018;31(8):785–98.
- [38] Ding J, et al. Thermo-mechanical analysis of Wire and Arc Additive Layer Manufacturing process on large multi-layer parts. *Computational Materials Science* 2011;50(12):3315–22.
- [39]. D. Ding, Z. Pan, D. Cuiuri, H. Li, A practical path planning methodology for wire and arc additive manufacturing of thin-walled structures, *Robot. Comput. Integr. Manuf.* 34 (2015) 8–19, <https://doi.org/10.1016/j.rcim.2015.01.003>.
- [40]. Z. Pan, D. Ding, B. Wu, D. Cuiuri, H. Li, J. Norrish, Arc welding processes for additive manufacturing: a review, *Trans. Intell. Weld. Manuf.* (2018) 3–24, [https://doi.org/10.1007/978-981-10-5355-9\\_1](https://doi.org/10.1007/978-981-10-5355-9_1).
- [41]. P. Singh, D. Dutta, Multi-direction slicing for layered manufacturing, *J. Comput. Inf. Sci. Eng.* 1 (2001) 129–142, <https://doi.org/10.1115/1.1375816>.

- [42]. D. Jafari, T.H.J. Vaneker, I. Gibson, Wire and arc additive manufacturing: opportunities and challenges to control the quality and accuracy of manufactured parts, *Mater. Des.* 202 (2021), 109471, <https://doi.org/10.1016/j.matdes.2021.109471>.
- [43]. Z. Pan, D. Ding, B. Wu, D. Cuiuri, H. Li, J. Norrish, Arc welding processes for additive manufacturing: A review, in: S. Chen, Y. Zhang, Z. Feng (Eds.), *Transactions on Intelligent Welding Manufacturing*. Transactions on Intelligent Welding Manufacturing, Springer, Singapore, 2018, [https://doi.org/10.1007/978-981-10-5355-9\\_1](https://doi.org/10.1007/978-981-10-5355-9_1).
- [44]. D. Ding, Z. Pan, D. Cuiuri, H. Li, S.V. Duin, Advanced design for additive manufacturing: 3D slicing and 2D path planning, *New Trends in 3D Printing*, Igor V Shishkovsky, IntechOpen (2018), <https://doi.org/10.5772/63042>.
- [45]. S.C. Park, B.K. Choi, Tool-path planning for direction-parallel area milling, *Comput. Aided Des.* 32 (2000) 17–25.
- [46]. R. Farouki, T. Koenig, K. Tarabanis, J. Korein, J. Batchelder, Path planning with offset curves for layered fabrication processes, *J. Manuf. Syst.* 14 (1995) 355–368.
- [47]. H. Wang, P. Jang, J.A. Stori, A metric-based approach to two-dimensional (2D) tool-path optimization for high-speed machining, *Transactions-American Society of Mechanical Engineers, J. Manuf. Sci. Eng.* 127 (2005) 33.
- [48]. D. Ding, Z. Pan, D. Cuiuri, H. Li, A multi-bead overlapping model for robotic wire and arc additive manufacturing (WAAM), *Robot. Comput. Integr. Manuf.* 31 (2015) 101–110, <https://doi.org/10.1016/j.rcim.2014.08.008>.
- [49]. Effect of wire and arc additive manufacturing (WAAM) process parameters on bead geometry and microstructure Malcolm Dinovitzer, Xiaohu Chen, Jeremy Laliberte\* , Xiao Huang, Hanspeter Frei
- [50]. Ortega AG, Galvan LC, Mezrag B (2017) Effect of process parameters on the quality of aluminium alloy Al5Si deposits in wire and arc additive manufacturing using a cold metal transfer process. *Sci Technol Weld Join* 6:1743–2936.
- [51]. Su C, Chen X, Gao C, Wang Y (2019) Effect of heat input on microstructure and mechanical properties of Al-Mg alloys fabricated by WAAM. *Appl Surf Sci* 486:431–440.

## 9. APPENDIX

**A-1 To attain a sound and defect-less part for Wire-Arc Additive Manufacturing, welding process-parameters to be considered include –**

- Wire Feed Rate (kg/hr)
- Travel Speed (m/min)
- Arc-Current (Ampere)
- Flow Gas rate
- Path-Strategy
- Heat-Input ( $\text{J}/\text{mm}^2$ )

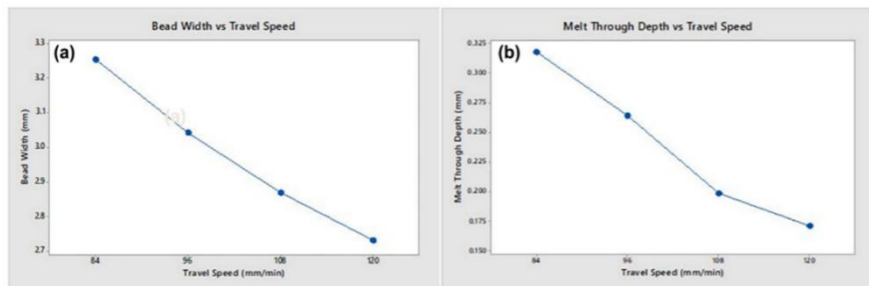


Figure A-I. Graphs between (a) Travel-speed vs bead-width, (b) Travel-speed vs melt-through depth

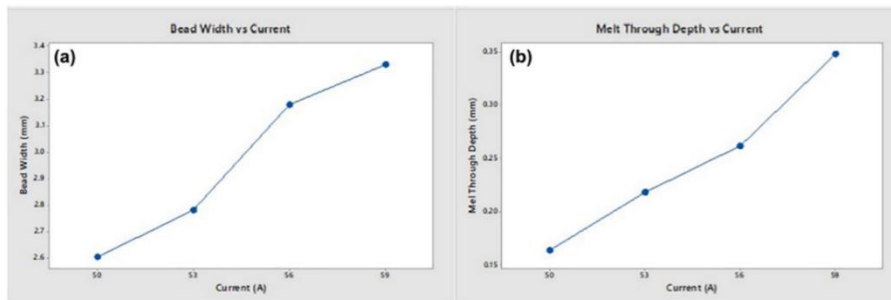


Figure A-II. Graphs between (a) Weld-current vs bead width, (b) Weld-current vs melt-through depth

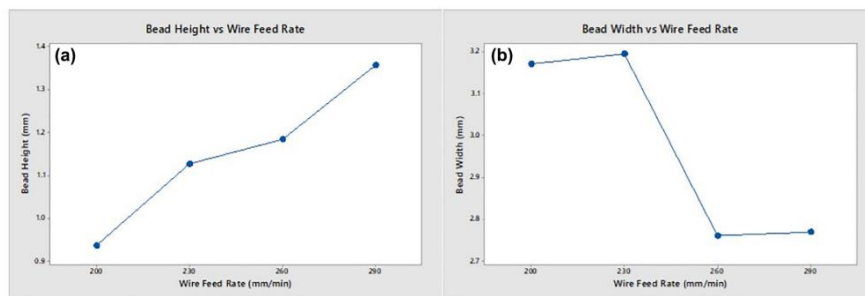


Figure A-III. Graphs between (a) Wire-feed rate vs bead height, (b) Wire-feed rate vs bead width

## A-2 Life Cycle of a WAAM part

specimen preparation through Wire-Arc Additive Manufacturing have three crucial steps:

- i. Process-planning,
- ii. Metal/Alloy deposition, &
- iii. Post-treatment

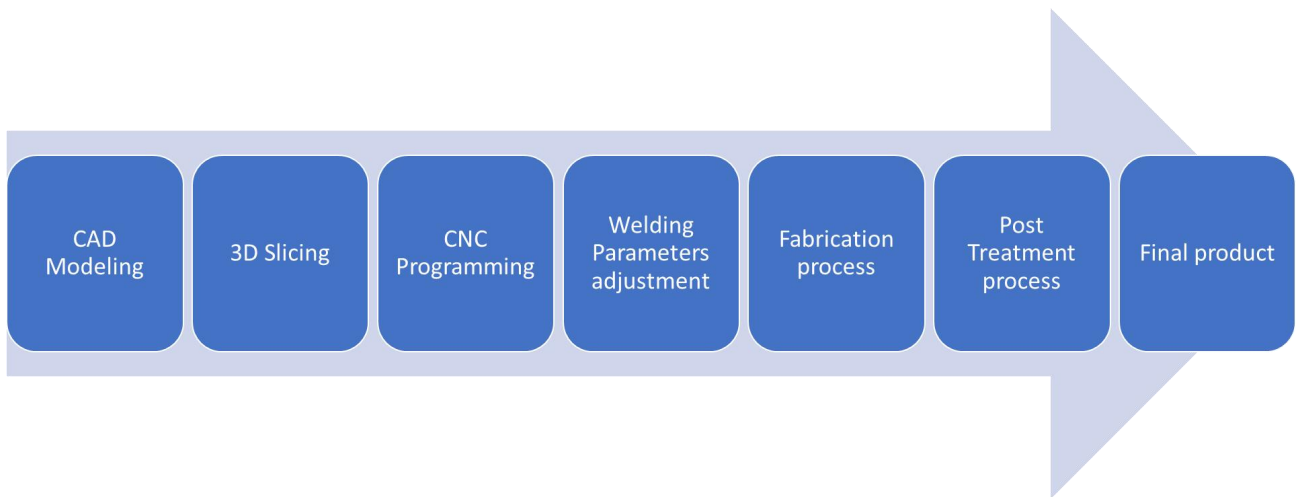


Figure A-IV. Life Cycle of a WAAM part